Utah State University

DigitalCommons@USU

All Graduate Theses and Dissertations | Graduate Studies

5-2013

Parallel Heat Transport in Magnetized Plasma

Mukta Sharma
Utah State University

Follow this and additional works at: https://digitalcommons.usu.edu/etd

 Part of the Plasma and Beam Physics Commons

Recommended Citation

Sharma, Mukta, "Parallel Heat Transport in Magnetized Plasma" (2013). *All Graduate Theses and Dissertations*. 1470.
https://digitalcommons.usu.edu/etd/1470

This Thesis is brought to you for free and open access by the Graduate Studies at DigitalCommons@USU. It has been accepted for inclusion in All Graduate Theses and Dissertations by an authorized administrator of DigitalCommons@USU. For more information, please contact digitalcommons@usu.edu.



PARALLEL HEAT TRANSPORT IN MAGNETIZED PLASMA

by

Mukta Sharma

A dissertation submitted in partial fulfillment
of the requirements for the degree

of

DOCTOR OF PHILOSOPHY

in

Physics

Approved:

Eric D. Held Major Professor	W. Farrell Edwards Committee Member
D. Mark Riffe Committee Member	James T. Wheeler Committee Member
Joseph Koebbe Committee Member	Mark R. McLellan Vice President for Research and Dean of the School of Graduate Studies

UTAH STATE UNIVERSITY
Logan, Utah

2012

Copyright © Mukta Sharma 2012

All Rights Reserved

ABSTRACT

Parallel Heat Transport in Magnetized Plasma

by

Mukta Sharma, Doctor of Philosophy

Utah State University, 2012

Major Professor: Dr. Eric D. Held
Department: Physics

A code that solves the coupled electron drift kinetic and temperature equations has been written to study the effects of collisionality and particle trapping on temperature equilibration along magnetic field lines. A Chapman-Enskog-like approach is adopted with the time-dependent distribution function written as the sum of a dynamic Maxwellian and a kinetic distortion expanded in Legendre polynomials. The drift kinetic equation is solved on a discrete grid in normalized speed, and an FFT algorithm is used to treat the one-dimensional spatial domain along the magnetic field. The dependence of the steady-state temperature on collisionality and magnetic well depths is discussed in detail. As collisionality decreases (increasing background temperature), temperature variations decrease. As magnetic well depth increases (at fixed collisionality), temperature variations along the field line increase.

(86 pages)

PUBLIC ABSTRACT

Parallel Heat Transport in Magnetized Plasma

by

Mukta Sharma, Doctor of Philosophy

Utah State University, 2012

A huge global increase in energy use is inevitable, so there is an urgent need to seek cleaner ways of producing energy on large scales. Fusion is the energy source of the universe and a promising way to fulfill energy needs of mankind for many centuries to come. It offers important advantages as a safe, sustainable, and environmentally friendly source of energy. The International Thermonuclear Experimental Reactor (ITER) aims to demonstrate magnetic fusion is an energy source of the future. The goal of ITER is to produce 500 MW of fusion power given 50 MW of input power—or ten times the amount of energy put in. The plasma in ITER is contained in a doughnut-shaped magnetic confinement device called a tokamak. It is important to understand heat transport parallel to the magnetic field in devices like this, since this can lead to degradation in heat confinement or drive instabilities that can cause the plasma to disrupt. This research contributes to our understanding of the underlying physics involved in parallel transport. Using a computer code, we solve the equations describing the plasma and calculate the parallel electron heat flow for different collisionality regimes. We also investigate the effect of magnetic wells on parallel electron heat flow.

To My Family

ACKNOWLEDGMENTS

First of all, I would thank God for fulfilling my dreams. I consider myself to be one of the luckiest graduate students because I had an opportunity to work with my advisor, Dr. Eric D. Held. Whatever I know about plasma physics, I owe to him. He has an immense role in igniting and shaping my interest in a field that I entered with a blank page. I do not think a simple thank you could do justice to his role in helping me to grow, not just as a student, but also as a person. I hope I make him proud by putting whatever he has taught me to good use throughout my life.

I'm so thankful to all my committee members, Dr. James Wheeler, Dr. Farrell Edwards, Dr. Mark Riffe, and Dr. Joseph Koebbe, for their encouragement and valuable time. I am especially grateful to Dr. Riffe for giving me an opportunity to work with him and learn so much from him. I would also like to thank Dr. Jeong-Young Ji for his useful suggestions in my research.

I'm so very grateful to Karalee, her motherly warmth and smile take all my worries away. I thank all my friends for their support all these years. Thank you Niti, Udit, and Rachayita for always being there for me. You guys are such great listeners.

I give great thanks to my family, especially to my husband. This long journey would be almost impossible to finish if it was not for my husband. It was with his support, encouragement, and love that I have made progress over the last so many years of my life. They say that behind every successful man there is a woman, but I am so blessed and proud to say that behind my success it is you, Kripa. I will be always indebted to my loving parents for being there for me and letting me come here, so far away from them, to fulfill my dreams. Love you Mummy and Papa. I'm also thankful to my in-laws for their support and patience. I am also grateful to my little kiddos, Prithika and Aarush, for their unconditional love. At the end of the day it is the smile on their faces that makes it all worthwhile.

I also want to thank Department of Physics for giving me an opportunity to work as a

teaching assistant. I am also thankful to US DOE for generously supporting this research.

Mukta Sharma

CONTENTS

Page

ABSTRACT iii

PUBLIC ABSTRACT iv

ACKNOWLEDGMENTS vi

LIST OF FIGURES x

CHAPTER

1. INTRODUCTION 1
   - 1.1 Overview 2
   - 1.2 Charged particle motion 6

2. COMPUTATION OF PARALLEL HEAT FLOW CLOSURE 10
   - 2.1 Fluid description of plasma 10
   - 2.2 Plasma kinetic equation 12
   - 2.3 The Lorentz collision operator 14
   - 2.4 Chapman-Enskog Drift Kinetic Equation 16
   - 2.5 Novel approach to solving the CEL-DKE 20
   - 2.6 The evolution of temperature 21
   - 2.7 Numerical Solution of the coupled F and T equations 22

3. RESULTS WITHOUT $|B|$ WELLS 26
   - 3.1 Convergence of the Legendre polynomial expansion 26
   - 3.2 Convergence of the speed representation 30
   - 3.3 Heat flow in different collisionality regimes without magnetic wells .. 35
   - 3.4 Distribution function in different collisionality regimes 38

4. RESULTS WITH MAGNETIC WELLS 44
   - 4.1 $q_{||}$ in the presence of magnetic wells for various collisonality regimes 45
   - 4.2 Distribution function in different collisionality regimes with $|B|$ effects 51
   - 4.3 Comparison of linear vs. nonlinear $|B|$ results 56

5. CONCLUSIONS AND FUTURE WORK 59
   - 5.1 Summary of the results 59
   - 5.2 Future work 62

REFERENCES 65

APPENDIX 67

A.1 Properties of Legendre polynomials 68
A.2 Definition of Laguerre polynomials 68
A.3 Derivation of |B| coupling terms 69

CURRICULUM VITAE 71

LIST OF FIGURES

Figure — Page

1.1 Poloidal cross section showing the poloidal projection of the trapped banana orbit 7

1.2 Temperature gradient scale length compared to the magnetic scale length for the ordering used in Held 8

1.3 The maximal ordering used in this dissertation permits the arrangement shown above with $L_B \sim L_T$ 9

3.1 Plot shows convergence of the standard deviation in temperature, σ_T, in the nearly collisionless limit as Legendre polynomials are added to the expansion 27

3.2 Convergence of the standard deviation in temperature, σ_T, in the collisional limit as Legendre polynomials are added to the expansion 28

3.3 Relative error, ε_{σ_T}, of the standard deviation in temperature, defined in Eq. (3.2) in the nearly collisionless limit 29

3.4 Convergence of the standard deviation in temperature, σ_T, in the collisional limit as speed points are added to the expansion 31

3.5 Relative error, ε_{σ_T}, of the standard deviation in temperature defined in Eq. (3.2) as a function of the number of speed grid points, n_s 32

3.6 Check for the convergence of the standard deviation in temperature, σ_T, in the nearly collisionless regime as speed points are added to the expansion . 33

3.7 Relative error, ε_{σ_T}, of the standard deviation in temperature in the nearly collisionless regime 34

3.8 Variation in normalized parallel electron heat flow and the normalized steady-state temperature 36

3.9 This plot for higher-temperature, lower-collisionality regimes looks similar to the one for higher collisionality, but with a smaller fluctuation in temperature. 37

3.10 This plot shows the standard deviation in temperature, σ_T, as collisionality varies 38

3.11 Contours of the distribution function at $s = 5$ in the collisionl regime with $L_v/L_s = 10^{-3}$ 40

3.12 Contours of the distribution function at $s = 5$, in the regime of intermediate collisionality with $L_v/L_s = 10^{-2}$ 42

3.13 Contours of the distribution function in the nearly collisionless regime with $L_v/L_s = 10$ 43

4.1 Plot shows variation in B and the spatially varying heat source, S, with a scale length of 100m 46

4.2 This plot shows the effect of the $\partial_L lnB$ term on temperature in the moderately collisional regime 47

4.3 The standard deviation in temperature, σ_T, versus change in magnetic well depth, δB, is plotted 49

4.4 The standard deviation in temperature, σ_T, versus change in magnetic well depth, δB, is plotted 50

4.5 Standard deviation in temperature in various collisionality regimes, with and without the $|\mathbf{B}|$ term in the F and T equations 52

4.6 Contours of the distribution function in the presence of magnetic wells with $\delta B = 0.4$ in the collisional regime, $L_v/L_s = 10^{-3}$ 53

4.7 As the frequency of collisions decreases with $L_v/L_s = 10^{-1}$, the effect of $|\mathbf{B}|$ can be observed in the contours of the distribution function for $s = 5$ . . 54

4.8 Contours of the distribution function at $s = 5$ in the nearly collisionless regime with $L_v/L_s = 10$ in the presence of magnetic wells of well depth $\delta B = 0.4$ 55

4.9 Plot shows gradient of temperature in presence of magnetic well with $\delta B =$ 0.4 in the nearly collisionless regime 56

4.10 Plot shows distribution function weighted by $v_{||}$ in the nearly collisionless regime 57

4.11 Plot of standard deviation in temperature in moderate collisionality regime versus magnetic well depth with and without the affect of $\partial_L lnB$ term in our kinetic equation 58

CHAPTER 1

INTRODUCTION

Long before man understood the concept of light and started harnessing energy for his needs, nature provided tremendous sources of light and energy by a majestical process known as fusion. Many decades ago, scientists understood the physics behind the transformation of hydrogen nuclei into helium atoms in the Sun and stars. This process releases huge amounts of energy. The first fusion experiments took place in the 1950s and resulted in a lot of information about the fusion process. After World War Two and the development of nuclear weapons, nuclear technologies, in general, increased. A major breakthrough occurred in 1968, when temperature levels in the KeV range and plasma confinement times in milliseconds were achieved for fusion in a doughnut-shaped magnetic confinement device called a tokamak. Many theoretical studies considered the tokamak as the most promising design, and research continues on various tokamaks around the world. The ITER device being built in France is an experimental reactor, which is expected to demonstrate an energy efficiency of 10 by confining hot plasma ($T \sim 10$ KeV, $n \sim 10^{20} m^3$) with confinement time of approximately four seconds generating fusion power at the 300-500 MW level.

The main objective of the controlled magnetized fusion program is the confinement of thermonuclear plasma by means of strong magnetic fields. Challanges to confining plasma have been plasma instability and transport. With advanced experiments, fast computing techniques, and more accurate theoretical work, many problems have been resolved. Heat conduction in the presence of a confining magnetic field of high-temperature experiments has been of major interest for scientists and researchers.

This dissertation focuses on a quantitative study of parallel electron heat flow along magnetic field lines. The plasma in most magnetic fusion devices is well magnetized, and here only the magnetized limit will be considered. In these devices, the core of a fusion plasma is nearly collisionless, whereas the colder edge region is (typically) moderately col-

lisional; therefore, both high and low collisionality are of interest. Here collisionality refers to the importance of binary Coulomb collision events between charged particle species in our plasma, which we will assume is perfectly ionized. In this research, an analytical and computational framework is developed for calculating the conductive electron heat flow, $q_{||}$, parallel to the direction of the confining magnetic field, **B**. This heat flow will be used to close the electron temperature equation for plasmas of arbitrary collionality. The macroscopic fluid description of plasma is extended by using kinetic theory. Specifically, a code that solves the coupled electron drift kinetic and temperature equations has been written to study the effects of collisionality and particle trapping in magnetic wells on temperature equilibration along magnetic field lines. Parallel computation is used to quickly determine the steady-state, transport equilibrium that indicates the effect on temperature and heat flow due to the presence of magnetic wells in different collisionality regimes.

In this work a Chapman-Enskog-like (CEL) approach is adopted with the time-dependent distribution function written as the sum of a dynamic Maxwellian and a kinetic distortion expanded in Legendre polynomials. The CEL approach has been used previously by Chang and Callen [1, 2] and Wang and Callen [3] to develop hybrid fluid/kinetic models and obtain transport coefficients. The drift kinetic equation, which is the magnetized limit of the plasma kinetic equation, is solved on a discrete grid in normalized speed and an expansion in Fourier series is used to treat the one-dimensional spatial domain along the magnetic field. The dependence of the steady-state temperature on collisionality and magnetic well depths is discussed in detail.

1.1 Overview

The state of an ionized plasma can be approximately described by using a fluid description in terms of macroscopic quantities like density, momentum, and energy for each species of charged particles. However, the fluid equations are not closed. Kinetic theory

is used to describe plasma in terms of the particle velocity distribution function, $f_s(\mathbf{x},\mathbf{v},t)$, where f_s is the exact microscopic phase space density of plasma species s, at point $\mathbf{x}$, with velocity $\mathbf{v}$, at time t. For simplicity, the subscript s will be dropped.

The fluid equations can be closed by calculating higher-order velocity-weighted moments of f, and thus getting the desired relationships between known quantites, like denstity, n, flow velocity, V, temperature, T, and the unknown quantites, such as the viscosity tensor, Π, and the conductive heat flow, $\mathbf{q}$. A few low-order velocity moments of the distribution function, f, are

number density, $n \equiv \int d^3v\, f$,

flow velocity, $n\mathbf{V} \equiv \int d^3v\, \mathbf{v} f$,

temperature, $nT \equiv \int d^3v\, \frac{m\mathbf{v}'}{3} f$, with the relative velocity $\mathbf{v}' \equiv \mathbf{v} - \mathbf{V}$,

and conductive heat flux, $\mathbf{q} \equiv \int d^3v\, \mathbf{v}' \frac{m\mathbf{v}'^2}{2} f$.

All these fluid moment properties are in general functions of spatial position, $\mathbf{x}$, and time, t, that is, $n = n(\mathbf{x},t)$. Details about the fluid equations are given in section 2.1 of Chapter 2.

The conductive heat flux, $\mathbf{q}$, is the random flow of thermal energy density. The theory of classical transport in magnetized plasma due to Coulomb collisions was established by Landshoff [4], Spitzer and Harm [5], Rosenbluth and Kaufman [6] and finally formulated by Braginskii [7]. In 1965, Braginskii derived the form of the heat flux parallel to a magnetic field, $q_{||}$, for collisional plasma (it is typical to term plasmas satisfying the short mean-free-path condition as collisional). His form was diffusive and proportional to the local parallel temperature gradient, $\hat{\mathbf{b}} \cdot \nabla T = \nabla_{||} T$. Here $\hat{\mathbf{b}} \equiv \frac{\mathbf{B}}{B}$, is the unit vector along $\mathbf{B}$. For the case of electrons,

$$q_{||e} \;=\; -\kappa_{||}(T_e)\nabla_{||}T_e = -3.16\frac{n_e T_e \tau_e}{m_e}\nabla_{||}T_e, \tag{1.1}$$

where $\tau_e = \frac{3}{4}\sqrt{\frac{m_e}{2\pi}}\frac{T_e^{3/2}}{\lambda e^4 Z^2 n_e}$ is the electron collison time, n_e and m_e are the electron density and mass, respectively, λ is the Coulomb logarithm, T_e is the electron temperature in eV, and $\kappa_{||}$ is the conductivity.

Comparing $\kappa_{||}$ in plasmas with the thermal conductivity in metals, in both the cases κ depends on the temperature. In pure metals, the electrical resistivity often increases proportional to temperature, and thermal conductivity tracks electrical conductivity. This behavior is given by the Wiedemann-Franz Law, which states that the ratio of the thermal conductivity to the electrical conductivity of a metal is proportional to the temperature, $\frac{\kappa}{\sigma} \propto T$, where σ is the electrical conductivity and $\frac{1}{\sigma}$ is the resistivity.

Unlike the electrical resistivity of metals, the resistivity of a fully ionized plasma varies inversely with $T^{3/2}$. As the temperature of a plasma is raised, its resistivity drops rapidly. Plasmas at very high temperatures have negligible resistance and thus are highly conducting. The electrical conductivity in plasma, $\sigma \propto T^{3/2}$.

As plasmas are heated, they become less collisional and the parallel thermal conductivity increases rapidly $\kappa_{||} \sim T^{5/2}$. Braginskii's theory works only in highly collisional regimes where the temperature $T \leq 30$ eV. Since present-day high-temperature fusion experminents operate in a regime where collisions are infrequent, there have been attempts to calculate the parallel heat flow closure in the collisionless limit, as well. In particular, Hammett and Perkins [8] proposed a collisionless heat flux, which involves kinetic free-streaming of electrons along magnetic field lines :

$$q_{||}(L') = \frac{n_e v_T}{\pi^{3/2}} \int_0^\infty dL \frac{T(L'-L) - T(L'+L)}{L/2} \tag{1.2}$$

.

Here L is the coordinate along the magnetic field. This form, too, is often unsatisfactory in

practice because it is only approximate in moderate collisionality regimes and it does not map onto the collisional version.

In magnetized plasmas, the Larmor radii, $\rho \equiv \frac{mv_\perp}{qB}$, are much smaller than the scale length of variations in quantities, such as fluid variables. Here $v_\perp$is the velocity perpendicular to the magnetic field. For such plasmas, the Larmor frequency, $\Omega \equiv eB/m \approx 10^{10}$ for electrons, which quantifies the frequency of particle gyration around magnetic field lines, is much larger than any other characteristic frequency. Also, the dominant parallel closure moments, which should capture all collisionality regimes are defined as [1]:

$$\pi_{||} = m \int d^3v (v_{||}^2 - \frac{v_\perp^2}{2}) f, \tag{1.3}$$

$$q_{||} = -T \int d^3v (\frac{5}{2} - \frac{v^2}{v_T}) v_{||} f. \tag{1.4}$$

Here the parallel stress tensor, $\Pi_{||} \equiv (\hat{\mathbf{b}}\hat{\mathbf{b}} - \mathbf{I}/\mathbf{3})\pi_{||}$, and the distribution function, f, come from the solution of a kinetic equation that emphasizes the parallel dynamics and retains a maximal ordering between parallel gradient scale lengths and collision lengths. Work by Held [9] provides an integral form for parallel ion viscous stress $\Pi_{||}$ and an analogous form for $q_{||}$ in a uniform magnetic field [10]. A unified closure for the conductive electron heat flux along an inhomogeneous magnetic field lines was also derived for arbitrary collisionality by Held [11]. The closure was in the form of a generic integral operator involving the electron temperature variation along a magnetic field line,

$$q_{||}(L) = \int_0^\infty dL' [T(L-L') - T(L+L')] \frac{\partial K}{\partial (lnL')}, \tag{1.5}$$

where the kernel, $K(L')$, contains information regarding the collisional effects of trapped and untrapped particles. This was derived for the case when electron collision lengths are long compared to the length of magnetic wells in which electrons can get trapped. In

this dissertation, we describe a numerical solution to the problem of heat flow along an inhomogeneous magnetic field, where sinusoidal variations in the magnetic field strength $|B|$ exists, making no assumptions about the ordering of various terms in kinetic equation. Before discussing this solution, we first describe the basics of charged particle motion along an inhomogeneous magnetic field.

1.2 Charged particle motion

In a uniform magnetic field, a charged particle gyrates around a magnetic field line and the guiding center of the particle's orbit moves with constant velocity along the field line. In a tokamak, the nonuniformity of the magnetic field leads to drifting of the guiding center. Since the toroidal magnetic field strength B_T is proportional to $1/R$, where R is the major radius of the tokamak (Fig. 1.1), the field is smaller on the outside of the torus. Particles in this region having a small velocity parallel to magnetic field undergo a magnetic mirror reflection as they move along field lines into the region of higher field. In the absence of collisions the particles are trapped in the low field region, bouncing back and forth between the turning points. The mirror force responsible for trapping is $F = -\mu \nabla B$, where $\mu = \frac{mv_\perp^2}{2B}$ is the approximately conserved magnetic moment for a particle with perpendicular velocity $\mathbf{v}_\perp$. Particles with large parallel velocity circulate continually around the torus and are called passing particles. In axisymmetric geometery, particle orbits can be viewed in the poloidal cross section at a fixed toroidal angle. The orbits of passing particles appear as simple closed curves surrounding the magnetic axis. However, the trapped particles reverse direction at bounce points causing a bounce motion, which in combination with radial drifts, produces orbits whose poloidal cross sections have a crescent shape as shown in Fig. 1.1.

At low collisionality, trapped particles dominate perpendicular transport, but do not contribute to parallel transport. When the collisionality is sufficiently low, the particles

complete several bounce orbits before having their velocity vector change substantially due to collisions, and the plasma is said to be in the banana regime based on the shape of the trapped orbits projected onto the poloidal plane.

In this low-collisionality regime, averaging the kinetic equation for electrons over these bounce orbits leads to a simpler equation to solve. In this work, we do not perform this average and hence, obtain results for parallel heat transport for a wider range of plasma collisionality and magnetic geometries. Compared to the previous theory, temperature gradient scale lengths, $L_T \equiv (\nabla_{||} lnT)^{-1}$ were considered much greater than the magnetic scale lengths, L_B. In this research however, the magnetic and temperature scale lengths are ordered arbitrarily with respect to each other (Figs. 1.2-1.3).

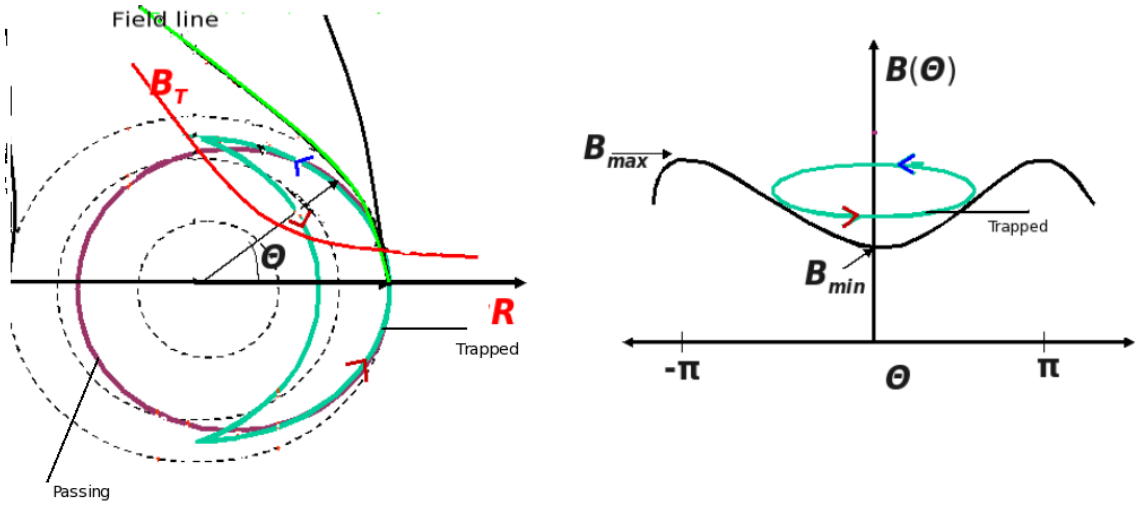


FIG. 1.1. Poloidal cross section showing the poloidal projection of the trapped banana orbit. There are two types of particles, passing and trapped. The toroidal magnetic field strength, B_T, varies inversely with the major radius, R. As the particle goes from the outer region towards the inner region, it faces a stronger magnetic field, and a particle having small velocity parallel to the magnetic field gets trapped in banana orbits.

Before continuing, we present an outline of the remaining chapters. In Chapter 2, we describe a novel treatment of the drift kinetic equation (DKE) and highlight the term, which describes the effect of magnetic field wells ($|B|$) on the heat flow closure. The closure problem is discussed, and the fluid model and kinetic approach to solve for the distribution function to obtain the closure are presented. We also describe the Lorentz collision operator used in this reasearch and how time-dependent effects are included. In Chapter 3, we present convergence studies for 2D velocity space. Results of heat flow in different collisionality regimes without the effect of the |B| term in the kinetic equation are also presented. Chapter 4 focuses on the effects of magnetic wells on the heat flow, in different collisionality regimes. Comparisions are made for the results obtained by using linear versus nonlinear |B| terms. Chapter 5 provides a general overview of the analytical and computational work done here and summarizes the key physics results obtained. Future work to investigate additional transport properties is also discussed.

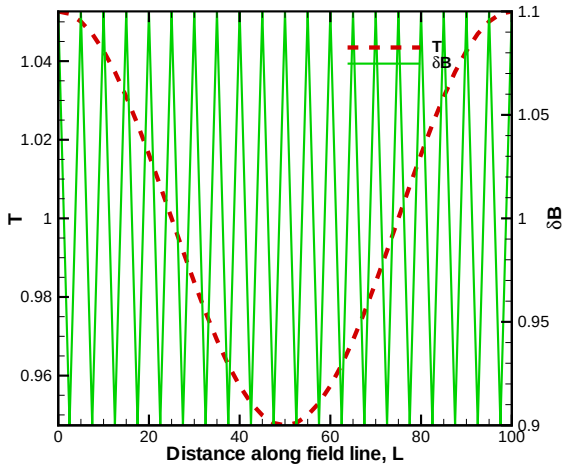


FIG. 1.2. Temperature gradient scale length compared to the magnetic scale length for the ordering used in Held [11]. This required $L_B \ll L_T$ as shown above.

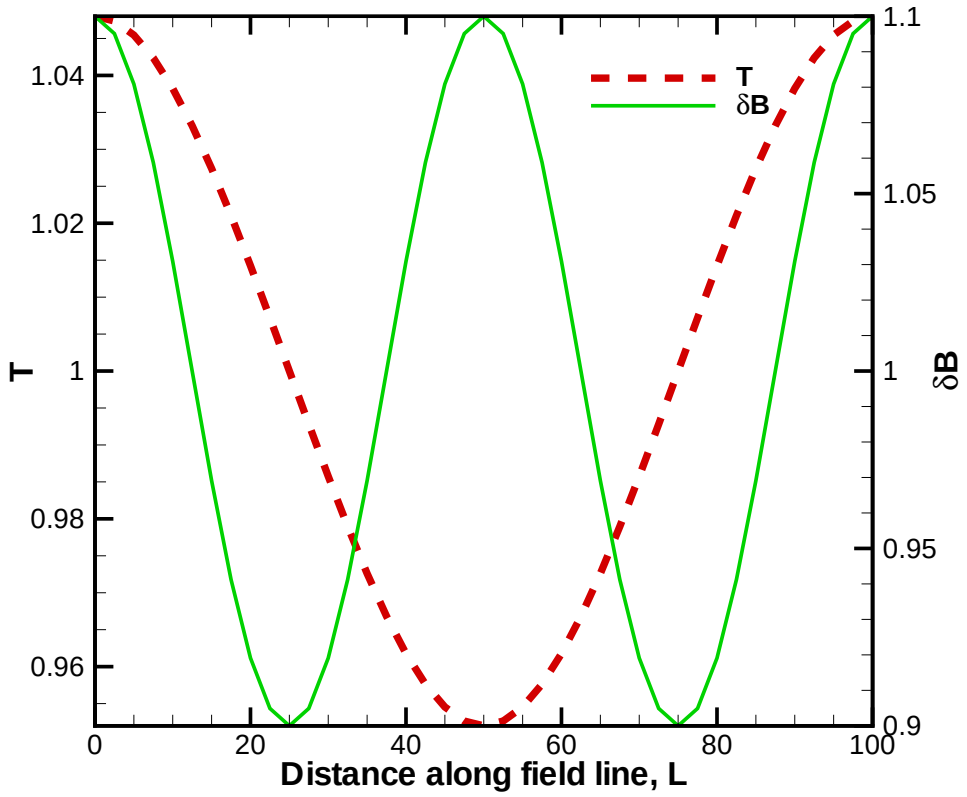


FIG. 1.3. The maximal ordering used in this dissertation permits the arrangement shown above with $L_B \sim L_T$.

CHAPTER 2

COMPUTATION OF PARALLEL HEAT FLOW CLOSURE

In this chapter, a numerical method for computing the heat flow parallel to the magnetic field is explained. In Section 2.1 we describe the plasma as a fluid and explain the transport equations. Section 2.2 discusses the time evolution of the distribution function, described by the plasma kinetic equation. A wide range of collision operators with varying degree of difficulty and accuracy have been used over several decades. Most prominent is the original form proposed by Boltzmann, which allows for hard (large-angle) scattering events, as well as small angle, Coulomb scattering events. Section 2 introduces the Coulomb collision operator used in this research, namely the limited Lorentz form of the Boltzmann operator frequently used for ionized plasmas. In section 2, the kinetic equation is converted into a drift kinetic equation (DKE) by averaging over the rapid gyromotion of electrons. The DKE highlights the dynamics parallel to the direction of the magnetic field. In section 2, we rewrite the DKE upon expanding the distribution function in terms of Legendre polynomials. Section 2 describes the numerical methods used to solve our coupled system of equations and how the closure is obtained for determining the parallel heat flow.

2.1 Fluid description of plasma

A number of analytical approaches have been developed to study plasmas, one of them being the fluid description [12]. The first step in the analytical fluid approach is to derive the governing system of equations, which deal with the macroscopic properties of the fluid. There are many ways to do this [13]. The five-moment method adopted in this work describes the time evolution of the density, n, flow velocity, $\mathbf{V}$, and temperature, T, and includes the effect of collisional friction, $\mathbf{R}$, collisional heating, Q, heat conduction, $\mathbf{q}$, and stress, Π, for each species.

The equation for density is

$$\frac{\partial n}{\partial t} + \nabla \cdot n\mathbf{V} \;=\; 0. \tag{2.1}$$

At a fixed position, evolution in the plasma density is caused either by advection of the species ($\mathbf{V} \cdot \nabla n$) or by compression of the flow ($n\nabla \cdot \mathbf{V}$). The first two terms on the right give the average force density on the species that results from the Lorentz force $[en(\mathbf{E} + \mathbf{v} \times \mathbf{B})]$ on the charged particles. The next two terms represent the force per unit volume on the species that results from the isotropic pressure, p, and the anisotropic stress, Π. The $\mathbf{R}$ term represents the frictional force density on a species due to Coulomb collisional relaxation of its flow, $\mathbf{V}$, toward the flow velocities of other species of charged particles in the plasma.

The equation for temperature is

$$\frac{3}{2} n \left(\frac{\partial}{\partial t} + \mathbf{V} \cdot \nabla \right) T \;=\; -p\nabla \cdot \mathbf{V} - \Pi : \nabla \mathbf{V} - \nabla \cdot \mathbf{q} + Q. \tag{2.2}$$

The temperature, T, of a plasma species evolves due to adiabatic compression or expansion ($-p\nabla \cdot \mathbf{V}$), the divergence of the conductive heat flux ($-\nabla \cdot \mathbf{q}$), dissipation due to flow-gradient-induced stress ($-\Pi : \nabla \mathbf{V}$) and collisional energy exchange (Q), between plasma species.

Equations (2.1)-(2.2) represent, respectively, the conservation of particles, momentum, and energy. They describe how these quantities move about (i.e., are transported) in the plasma. Each moment is coupled to the next higher one. Density evolution depends upon velocity. Evolution of velocity depends upon pressure gradients ($\nabla p = \nabla nT$) and stress, and so on. Thus, the density, flow, and temperature equations require higher closure moments, namely the conductive heat flux, $\mathbf{q}$, the stress tensor, Π, the collisional friction force density, $\mathbf{R}$, and the collisional energy exchange, Q, in order to be closed.

The system of fluid equations can be closed in number of ways. Accurate closure has

proven beneficial for describing a wide varity of observed phenomema in plasma [14, 15]. One simple way to close fluid equations is by brute force truncation, simply ignore the higher order moments. Another method of closing fluid equations is based on rigorous exploitation of small parameters, called asymptotic closure. This method is more systematic, and provides an estimate of the error involved. The closure scheme developed here involves a hybrid fluid/kinetic approach [1, 2]. The classic example of this approach is the Chapman-Enskog theory of a gas dominated by collisions [16], details of it are provided in section 2.4 of this chapter.

2.2 Plasma kinetic equation

Plasma kinetic theory, among other things, provides a method of investigating the influence of collisions among plasma particles. It also treats effects like free-streaming and magnetic trapping, which play an important role in determining transport in magnetized plasmas. Rather than tracking the position and velocity of every individual particle in the plasma, which would be a daunting task, kinetic theory provides for each particle species a distribution function, $f(\mathbf{x}, \mathbf{v}, t)$, which represents the probable number of particles that will be found at time t in an elemental volume of six-dimensional configuration space, $d\mathbf{x}d\mathbf{v}$. The total number density (number of particles per unit volume) can be obtained by taking the integral of f over velocity space. Similarly, the bulk flow may be computed by weighting the velocity space integral of f by the particle velocity, $\mathbf{v}$. These two lowest order moments give the desired constitutive relations: expressions for the charge density and current density needed to close Maxwell's equations. The distribution for each species is determined by a single partial differential equation in the six variables $\mathbf{x}$, $\mathbf{v}$, and time t.

The original kinetic model is the Boltzmann transport equation [17, 18]. It achieved great success in the late nineteenth century by accurately describing the kinetics of molecular gases, and presents a natural starting point for a plasma kinetic equation. The Boltz-

mann equation considers only binary particle interactions; that is, it assumes at a microscopic level each particle interacts with at most one other particle at a time [19]. It is given by

$$\frac{\partial f}{\partial t} + \mathbf{v} \cdot \nabla f + \mathbf{a} \cdot \nabla_{\mathbf{v}} f = C(f), \tag{2.3}$$

where $C(f)$ is the collision operator and $\mathbf{a}$ is the acceleration. If the collision operator is neglected, and the acceleration is given by the Lorentz force, then the Boltzmann equation is referred to as the Vlasov equation [20]. Eq. (2.3) describes the evolution of the distribution function, $f(\mathbf{x}, \mathbf{v}, t)$, for particles of each species in the plasma. It provides a statistical description of plasma dynamics in configuration space. The symbol ∇ stands for the gradient in space and the symbol $\nabla_{\mathbf{v}} = \frac{\partial}{\partial \mathbf{v}}$ stands for the gradient in velocity space.

Solving the Boltzmann equation is extremely difficult. Much work has been done to obtain analytical solutions for simple cases. Hilbert was first to obtain a result expressing the solution of the Boltzmann equation as a series expansion [21]. Chapman and Enskog [16] obtained a series solution valid for dense collisional gases. Grad [13] developed a systematic method of expanding the solution of the Boltzmann equation in a series of orthogonal polynomials.

In Eq. (2.3), $\mathbf{v} \cdot \nabla f$, refers to the free streaming of particles. For many laboratory and astrophysical plasmas, the Lorentz acceleration dominates and is given by

$$\mathbf{a} = \frac{e}{m}(\mathbf{E} + \mathbf{v} \times \mathbf{B}), \tag{2.4}$$

where e and m are the particle charge and mass, respectively. It is the magnetic portion of the Lorentz force that acts on the particles and localizes them in the magnetic field, forcing them to approximately follow the field lines in magnetized plasmas. In the absence of an electric field, $\mathbf{E}$, the magnetic component of the Lorentz force acts to restrict the

motion of particles across **B**. As a result they execute localized gyro-orbits (characterized by very small gyroradii) around the magnetic field lines. The gyroradius is submillimeter for a 1keV electron gyrating in a 1T magnetic field. In steady state, the free streaming of particles ($\mathbf{v}\cdot\nabla f \approx \mathbf{v}_{||}\cdot\nabla f$) balances collisional effects and the thermodynamic drives associated with gradients in temperature, density and flow. The transit timescale associated with the free-streaming of particles is fast compared to resistive and transport timescales of fusion and astrophysical plasmas. As a result, this term, $\mathbf{v}\cdot\nabla f$, is difficult to treat generally. Special emphasis is made in this research to incorporate the effect of an inhomogeneous magnetic field, which is present in $\mathbf{v}\cdot\nabla f$ on the conductive heat flow, by treating this term using a novel method. Additional complication in solving Eq. (2.3) is provided by the collision operator, $C(f)$.

2.3 The Lorentz collision operator

Charged particles in fully ionized plasmas interact with each other primarily through binary Coulomb collision events. These collisions are important when describing diffusion, mobility, resistivity, and conductivity in a plasma. Coulomb collision effects cause diffusion and deceleration of a particle's velocity vector as it passes near individual charged background particles, and gets deflected by the electric force from them. Three properties of the Coulomb collision operator, (i) no particles are created or destroyed via Coulomb collisions, (ii) momentum, and (iii) energy is conserved, should be preserved when constructing numerical solutions to Eq. (2.3).

One of the simplest models with which we can approximate these Coulomb effects is the Lorentz collision model. It contains the basic effects of momentum loss and velocity-space diffusion. Its simplest form assumes the plasma consists of positively charged ions and negatively charged electrons. The background ions are considered infinitely massive (stationary) and randomly distributed in space. Hence the Lorentz collision operator de-

termines how the electron distribution function evolves due to collisions with one or more stationary, background ion species. The spatial position of the test particle is not significantly affected by collisions, which generate random, small kicks to a particle's velocity vector. Spatial scales are assumed to be larger than the Debye length, $\lambda_D = 10^{-4}$m, in a typical tokamak plasma. Time scales are assumed to be longer than the time required for a test particle to traverse a Debye sphere. There is also no energy exchange, and hence, no energy diffusion in this model.

For electrons, the form for the Lorentz scattering operator used in this research is

$$C(F) = L(F) = \frac{\nu_L(v)}{2} \frac{\partial}{\partial(\frac{v_\parallel}{v})} \left(1 - (\frac{v_\parallel}{v})^2\right) \frac{\partial F}{\partial \frac{v_\parallel}{v}}. \tag{2.5}$$

The above equation represents diffusion in pitch angle space, $\frac{v_\parallel}{v}$, where $v_{||} = \mathbf{v} \cdot \hat{\mathbf{b}}$ is the component of the velocity vector along the magnetic field and $v = |\mathbf{v}|$. The Lorentz speed-dependent collision frequency, ν_L, is [22]

$$\nu_L = \nu_{ei} + \nu_{ee} = \frac{\nu_{ee}}{s^3} \left[Z_{eff} + \phi(s) - G(s)\right], \tag{2.6}$$

where ϕ is the error function, $G = \frac{1}{2}\left(\frac{v_{Tj}}{v}\right)^2 (\phi - (\frac{v}{v_{Tj}})\phi')$, is a function first introduced by Chandrasekhar [23], ν_{ee} is the reference collision frequency, and $Z_{eff} = \sum_j n_j Z_j^2 / \sum_j n_j Z_j$, with the sum performed over all ion species. The collision frequency, ν_L, characterizes the time over which a particle's velocity vector scatters through 90^0 in pitch angle, due to multiple small-angle scattering events. The eigenfunctions of the Lorentz scattering operator are Legendre polynomials (see the Appendix), hence the operator, $L(F)$, can be written as

$$L(F) = -\frac{\nu_L(v)}{2} \sum_n n(n+1) F_n(\mathbf{x}, \mathbf{v}, t) P_n(\frac{v_{||}}{v}), \tag{2.7}$$

where $n(n+1)$ are the eigenvalues and the distribution function, F, has been expanded in Legendre polynomials, $F = \sum_n F_n P_n$. Orthogonality is applied (see the Appendix) as part of an effort to convert the PDE in Eq. (2.3) into a linear system of coupled ordinary differential equations.

2.4 Chapman-Enskog Drift Kinetic Equation

The fluid treatment of plasma is useful for characterizing large scale-length, slower plasma phenomena. However, as mentioned in section 2.1, serious extensions of the fluid model are required in order to fully understand some plasma behavior. Often these extensions come from the kinetic description of plasma. A practical approach is to use both the fluid and kinetic models, and combine them into a unified model. We develop a hybrid fluid/kinetic model for describing a magnetically confined plasma via a five moment Chapman-Enskog-like (CEL) procedure. This approach uses the density, n, flow, $\mathbf{V}$, and temperature, T, evolution equations, and recasts the plasma kinetic equation into a partial differential equation for the kinetic distortion, F, which evolves according to thermodynamic drives.

The fundamental idea of the Chapman-Enskog method is to suppose the distribution function evolves in time only, or primarily (to lowest order) as a result of changes in the fundamental parameters of the Maxwellian distribution function, $n(\mathbf{x},t)$, $\mathbf{V}(\mathbf{x},t)$, and $T(\mathbf{x},t)$:

$$f(\mathbf{x},\mathbf{v},t) \quad \rightarrow \quad f[\mathbf{x},\mathbf{v};n(\mathbf{x},t),\mathbf{V}(\mathbf{x},t),T(\mathbf{x},t)]. \tag{2.8}$$

In the CEL approach, we make the Ansatz the distribution is to lowest order a Maxwellian, with important corrections that will give rise to the parallel heat flux, $q_{||}$. In the original treatment of Chapman and Enskog, the ratio of mean-free-path to scale size provides a small parameter for systematic expansion of the kinetic equation. Here we relax that

assumption, and hence, refer to our approach as Chapman Enskog like. The Chapman-Enskog Ansatz [16] posits the distribution function, f, may be written as a sum of a dynamic Maxwellian f_M , which represents the physics of a fluid model, plus a kinetic distortion F:

$$f = f_M + F = n(\mathbf{x},t)\,(\frac{m}{2\pi T})^{\frac{3}{2}} exp\left(-\frac{mv'^2}{2T}\right) + F, \tag{2.9}$$

where $\mathbf{v}' \equiv \mathbf{v} - \mathbf{V}$ is the random velocity and the density, temperature and flow moments of f_M are n, T, and $\mathbf{V}$, respectively. The parallel heat flow moment of f_M vanishes, hence our expression for $q_{||}$, which is needed to close the temperature equation, depends strictly on the kinetic distortion, F, which is obtained by solving our approximate kinetic equation.

Substituting Eq. (2.9) into our plasma kinetic equation [Eq. (2.3)] leads to

$$\frac{\partial(f_M + F)}{\partial t} + \mathbf{v}\cdot\nabla(f_M + F) + \mathbf{a}\cdot\nabla_{\mathbf{v}}(f_M + F) = C(f_M + F), \tag{2.10}$$

which may be written simply as

$$\frac{dF}{dt} - C(f_M + F) = -\frac{df_M}{dt}. \tag{2.11}$$

Here

$$\frac{d}{dt} = \frac{\partial}{\partial t} + \mathbf{v}\cdot\nabla + \mathbf{a}\cdot\nabla_{\mathbf{v}}, \tag{2.12}$$

is the total time derivative. Writing out the total time derivative explicitly for F terms yields

$$\frac{\partial F}{\partial t} + \mathbf{v}\cdot\nabla F + \mathbf{a}\cdot\nabla_{\mathbf{v}}F - C(F + f_M) = -\frac{df_M}{dt}. \tag{2.13}$$

The right side of the above equation can be written as

$$\frac{df_M}{dt} = \left(\frac{d\ ln(n)}{dt} + \left(\frac{mv'^2}{2T} - \frac{3}{2} \right) \frac{d\ ln(T)}{dt} + \frac{mv'^2}{T} \cdot \left(\frac{d\mathbf{V}}{dt} - \mathbf{a} \right) \right) f_M. \tag{2.14}$$

Equation (2.13) shows how the kinetic distortion, F, is driven by spatial and temporal variations of the fluid variables parameterizing f_M. In this research, F is obtained by solving an approximate form of Eq. (2.13). Taking the $q_{||}$ moment of F, we get the desired closure for the temperaure evolution equation.

In magnetized plasmas, it is possible to average Eq. (2.13) over the rapid gyromotion $\frac{e}{m}(\mathbf{v} \times \mathbf{B})$ because the frequency of gyromotion about the magnetic field, $\Omega = \frac{qB}{m}$, is higher than other frequencies of interest. Gyroaveraging reduces velocity space from three dimensions to two dimensions and highlights the dominant parallel dynamics of magnetized plasmas as mentioned in section 2 of this chapter.

Averaging over the rapid gyration of electrons about the magnetic field, ignoring acceleration effects due to an electric field, and assuming the magnitude of the flow $|\mathbf{V}|$ is small compared to the thermal speed, v_T, yields the lowest-order CEL drift kinetic equation (CEL-DKE) [1, 20]:

$$\begin{aligned} \frac{\partial F}{\partial t} + v_{||}\mathbf{b} \cdot \nabla F - \langle C(F + f_M) \rangle \quad = \quad & \overbrace{\frac{2}{3}\left(\frac{v^2}{v_T^2} - \frac{3}{2}\right)[\nabla \cdot \mathbf{q} - Q + \nabla \mathbf{V} : \Pi_{||}]\frac{f_M}{p}}^{(a)} \\ & + \overbrace{v_{||}(\mathbf{b} \cdot \nabla \cdot \Pi_{||} - R_{||})\frac{f_M}{p}}^{(b)} - \overbrace{\left(\frac{v^2}{v_T^2} - \frac{5}{2}\right)v_{||} \cdot (\nabla_{||} T)\frac{f_M}{T}}^{(c)} \\ & - \overbrace{\frac{m}{T}(\mathbf{bb} - \frac{\mathbf{I}}{3}) : \nabla \mathbf{V}(v_{||} - \frac{v_\perp^2}{2}) f_M}^{(d)}, \end{aligned} \tag{2.15}$$

where $\nabla_{||} = \hat{\mathbf{b}} \cdot \nabla$ is the gradient in the direction of the magnetic field. The over-braced term (a) in the above equation is due to heat conduction and viscous and collisional heat-

ing. Term (b) represents stress and collisional friction drives. Term (c) is the temperature gradient drive and term (d) is the flow gradient drive. Also, $\langle C(F+f_M)\rangle$ is the gyroaveraged collision operator, which for our purposes, is the Lorentz form given in Eq. (2.7).

In this research, we assume the magnitude of the flow velocity $|\mathbf{V}|$ to be small compared to the thermal velocity, $v_T = \sqrt{2T/m}$. We also ignore the stress, $\Pi_{||}$, flow gradient drive, $\nabla\mathbf{V}$, and collisional friction, $R_{||}$, drive in order to focus only on how parallel gradients in temperature, $\nabla_{||}T$, drive parallel conductive heat flow. Under these assumptions, Eq. (2.15) becomes

$$\frac{\partial F}{\partial t} + v_{\|}\mathbf{b}\cdot\nabla F - \langle C(F+f_M)\rangle = L_1^{\frac{3}{2}} v_{||}\nabla_{\|}T\frac{f_M}{T} - f_M L_1^{\frac{1}{2}}\frac{1}{T}\frac{\partial T}{\partial t}, \tag{2.16}$$

where $L_1^{3/2} = (\frac{5}{2} - s^2)$ and $L_1^{1/2} = (\frac{3}{2} - s^2)$ are Laguerre polynomials (see the Appendix), $s \equiv v/v_T$ is the normalized speed variable, and we have used our temperature evolution equation to rewrite term (a) in Eq. (2.15).

Again, Eq. (2.16) emphasizes the dominant parallel dyanmics of magnetized plasmas. The other important equation of interest, for calculating parallel heat transport, is the simplified temperature evolution equation [Eq. (2.2)]:

$$\frac{3}{2}n\frac{\partial T}{\partial t} = -\nabla\cdot q_{||}\hat{b} + S, \tag{2.17}$$

where S is a heat source which, for our purposes, varies spatially but is constant in time.

In this research, Eq. (2.16) and Eq. (2.17) are the two important coupled equations. They are advanced in time in order to study the temperature distribution along magnetic field lines, given a time-independent, spatially varying heat source, S.

2.5 Novel approach to solving the CEL-DKE

The evolution equation for F is a PDE in four independent variables, $\frac{v_{||}}{v}$ (pitch angle), s (normalized speed), L (distance along field line), and t. This couples to the T evolution equation, which has two independent varibles, L and t. We simplify the geometry by considering a 1-D periodic domain with $L\ \varepsilon\ [0, L_{max}]$.

As discussed earlier, we expand the kinetic distortion, F, as

$$F = \sum_{n=0}^{N} F_n(s,L,t) P_n\left(\frac{v_{||}}{v}(L)\right), \tag{2.18}$$

where P_n are Legendre polynomials parameterized by $\frac{v_{||}}{v}$. Here $\frac{v_{||}(L)}{v} = \pm\sqrt{1-\frac{\mu B(L)}{w}}$ with $w = \frac{1}{2}mv^2$, the kinetic energy and $\mu = \frac{mv_{\perp}^2}{2B}$, the magnetic moment. Here $\frac{v_{||}}{v} = \pm 1$ means there is no magnetic moment and $\frac{v_{||}}{v} = 0$ indicates all of the electron's energy is devoted to gyromotion.

Upon substituting the above expansion for F into Eq. (2.16), one must be careful to have the parallel gradient operator act on both the coefficients of the distribution function, F_n, and the Legendre polynomials, $P_n(\frac{v_{||}}{v})$:

$$\frac{\partial}{\partial t}\sum_{n=0}^{N} F_n P_n + v_{||}\mathbf{b}\cdot\sum_{n=0}^{N}\left[\left(\nabla F_n\right)P_n + F_n\left(\nabla P_n\right)\right] - \left\langle C\left(\sum_{n=0}^{N} F_n P_n + f_M\right)\right\rangle$$
$$= L_1^{\frac{3}{2}} v_{||}\nabla_{||} T\frac{f_M}{T} - f_M L_1^{\frac{1}{2}}\frac{1}{T}\frac{\partial T}{\partial t}. \tag{2.19}$$

Here, the term $\nabla_{||}P_n(\frac{v_{||}}{v})$ simplifies to (see the Appendix) :

$$\nabla_{||}P_n(\frac{v_{||}}{v}) = \left[\left(\frac{v_{||}}{v}\right)^2 - 1\right](\nabla_{||} lnB)P_n'\left(\frac{v_{||}}{v}\right). \tag{2.20}$$

Using the recurrence relations of Legendre polynomials

$$P_n'(\tfrac{v_{||}}{v}) = n\left(\frac{v_{||}}{v}\right)P_n - nP_{n-1}.$$

Substituting Eq. (2.20) into Eq. (2.19), multiplying by $P_m(\frac{v_{||}}{v})$, and integrating over $\int_{-1}^{1} d(\frac{v_{||}}{v})$ gives

$$\frac{\partial}{\partial t}\int_{-1}^{1} d(\tfrac{v_{||}}{v})P_m \sum_n F_n P_n + \int_{-1}^{1} d(\tfrac{v_{||}}{v})P_m\left(\frac{\nu_L(v)}{2}\sum_n n(n+1)\right)F_nP_n$$

$$+v\int_{-1}^{1} d(\tfrac{v_{||}}{v})P_m\frac{v_{||}}{v}\sum_n P_n\nabla_{||}F_n + v\int_{-1}^{1} d(\tfrac{v_{||}}{v})P_m\left(\frac{v_{||}}{v}\right)\sum_n\left[n\left(\frac{v_{||}}{v}\right)P_n - nP_{n-1}\right](\nabla_{||}lnB)F_n$$

$$= v\int_{-1}^{1} d(\tfrac{v_{||}}{v})P_m L_1^{\frac{3}{2}}\frac{v_{||}}{v}\nabla_{||}T\frac{f_M}{T} - \int_{-1}^{1} d(\tfrac{v_{||}}{v})P_m L_1^{\frac{1}{2}}\frac{\partial T}{\partial t}f_M. \quad (2.21)$$

Applying the orthogonality properties of Legendre polynomials yields a set of $N+1$ equations for the vector of coefficients, $\mathbf{F} = (F_0, F_{1,}..., F_N)$:

$$[\underline{\mathbf{I}}\partial_t + \frac{\nu_L}{2}\underline{\Gamma}]\mathbf{F} + \underline{\mathbf{A}}v\partial_L\mathbf{F} + \underline{\mathbf{M}}v(\partial_L lnB)\mathbf{F} = \delta_{l1}L_1^{\frac{3}{2}}v(\partial_L lnT)f_M - \delta_{l0}L_1^{\frac{1}{2}}(\partial_t lnT)f_m. \quad (2.22)$$

Here $\underline{\mathbf{I}}$ is the $N+1\times N+1$ identity matrix, $\underline{\Gamma}$ is diagonal with $n(n+1)$ in the n^{th} row and column and zeros elsewhere, $\underline{\mathbf{A}}$ represents the free-streaming coupling, and $\underline{\mathbf{M}}$ captures the effect of magnetic wells, which can trap particles. Both $\underline{\mathbf{A}}$ and $\underline{\mathbf{M}}$ come from the $v_{||}\mathbf{b}\cdot\nabla F$ term in Eq. (2.16). The vector $\mathbf{F}$ is made up of the expansion coefficients $F_n(s,L,t)$. The parallel derivative is written as $\nabla_{||} = \mathbf{b}\cdot\nabla = \partial_L$, where again, L is the coordinate along the magnetic field line, and δ_{ln} is the Kronecker delta, denoting the $\partial_t lnT$ drive appears only in the equation for F_0 and the $\partial_L lnT$ drive appears only in the F_1 equation.

2.6 The evolution of temperature

The temperature evolution equation can be written as

$$\frac{\partial T}{\partial t} = \frac{2}{3nT_0}(-\partial_L q_{||} + q_{||}\partial_L lnB + S), \tag{2.23}$$

where we have normalized temperature to a constant background temperature, T_0, which will be used to control the collisionality of the plasma. Here we have also used, $\nabla \cdot \frac{\mathbf{B}}{B} = \mathbf{B} \cdot \nabla \frac{1}{B} = -\frac{\mathbf{B}}{B^2} \cdot \nabla B = -\mathbf{b} \cdot \nabla lnB = -\partial_L lnB$. With the definition of F in Eq. (2.18), the parallel heat flow moment can be written as

$$q_{||} \;=\; -T \int d\mathbf{v} v_{||} L_1^{3/2} F = -T \frac{4\pi}{3} v_T^4 \int_0^\infty ds s^3 L_1^{3/2} F_1, \tag{2.24}$$

where our three dimensional velocity space has $d\mathbf{v} \rightarrow 2\pi s^2 ds\, d\left(\frac{v_{||}}{v}\right)$.

The terms $\underline{\mathbf{M}} v(\partial_L lnB)F$ in Eq. (2.22) and $q_{||}\partial_L lnB$ in Eq. (2.23) determine the effect on heat flow due to the inhomogeneous magnetic field. After the heat source, S, is switched on, the temperature evolves until the system reaches the steady state, $\frac{\partial T}{\partial t} = 0$. At that time, the flow of heat balances the spatially varying heat source, which satisfies $\int_0^{Lmax} dL\, S = 0$. In the absence of the $\partial_L lnB$ term, $\frac{\partial q_{||}}{\partial L} = S$ in steady state. In the presence of magnetic wells the steady-state form of Eq. (2.23) is $\frac{\partial q_{||}}{\partial L} - q_{||}\partial_L lnB = S$, and the heat source is balanced not only by the parallel heat flux, but also by the magnetic well term.

2.7 Numerical Solution of the coupled F and T equations

As we know, solving the kinetic equation numerically can be a daunting task. Therefore, in this research we use parallel computing to solve our time-dependent coupled system of equations. We use a discrete grid in the normalized speed variable, s, which allows for parallel computation over our radial coordinate in velocity space. The work is distributed over multiple processors, which communicate using MPI (Message Passing Interface) [24] in order to solve our coupled system of equations [Eqs. (2.22) and (2.23)] efficiently. We

also use finite differencing in time, and an efficient Fourier series representation in space, L. In this section, we give details about the various numerical and computational tecniques used to obtain the desired closure in this research.

2.7.1 Spatial representation using complex Fourier series

The spatial dependence of the coefficients, $F_n(s,L,t)$, can be represented using a complex Fourier series. The 1-D Fourier representation for the coefficients of the Legendre expansion used in this research is

$$F_n(s,L,t) = F_{n0}(s,t) + \sum_{m>0}^{m_{max}} [F_{nm}(s,t)e^{im\phi} + F^*_{nm}(s,t)e^{-im\phi}]. \tag{2.25}$$

Here $\phi = \frac{2\pi L}{L_{max}}$ is the phase angle. Similarly, $\partial_L lnB$ and T may be expanded as

$$\partial_L lnB = \sum_{m>0}^{m_{max}} (B_m e^{im\phi} + B^*_m e^{-im\phi}), \tag{2.26}$$

and

$$T = T_0 + \sum_{m>0}^{m_{max}} (T_m e^{im\phi} + T^*_m e^{-im\phi}). \tag{2.27}$$

Fourier series are useful in solving partial differential equations because they convert them into algebraic equations. A Fast Fourier Transform (FFT) is used to form nonlinear products and go between real (L) and Fourier (m) space.

Substituting Eqs. (2.25-2.27) into the equation for the evolution of the distribution function, Eq. (2.22), multiply by $\frac{e^{-im'\phi}}{2\pi}$ and integrating over $\phi\varepsilon[0,2\pi]$ ($L\varepsilon[0,L_{max}]$) yields

$$\begin{aligned}[\underline{\mathbf{I}}\partial_t + \frac{\nu_L}{2}\underline{\Gamma}]\mathbf{F}_{m'} + \left(\frac{2\pi}{L_{max}} im'\right)\underline{\mathbf{A}}v\mathbf{F}_{m'} + \underline{\mathbf{M}}v(\mathbf{F}B)_{m'} = \\ \delta_{l1}L_1^{\frac{3}{2}}v\left(\frac{2\pi}{L_{max}} im'\right)T_{m'}f_M - \delta_{l0}L_1^{\frac{1}{2}}(\partial_t T_{m'})f_m,\end{aligned} \tag{2.28}$$

where $\mathbf{F}_{m'} = (F_{0m'}, F_{1m'}, ..., F_{Nm'})$ and

$$(\mathbf{F}B)_{m'} = \frac{1}{2\pi}\int_0^{2\pi} d\phi\ e^{-im'\phi}\left[\mathbf{F}_0 + \sum_{m>0}^{m_{max}}(\mathbf{F}_m e^{-im\phi} + \mathbf{F}_m^* e^{-im\phi})\right] \left(\sum_{m''>0}^{m_{max}} B_{m''}e^{im''\phi} + B_{m''}^* e^{-im''\phi}\right). \tag{2.29}$$

The product of $\partial_L lnB$ and F in Eq. (2.22) is treated as a nonlinear term and a forward FFT is applied to this term, by which real space data is converted into Fourier harmonics, $(\mathbf{F}B)_{m'}$. The FFT of a two-dimensional array over the second dimension, for all points in the first dimension, is performed.

Similarly for temperature

$$\frac{\partial T_{m'}}{\partial t} = -\overbrace{\frac{8\pi}{9}v_T T_0 \int ds s^3 L_1^{3/2}(F_1 B)_{m'}}^{a} + \frac{2}{3nT_0}S_{m'} + \overbrace{\frac{8\pi}{9}v_T T_0 \int ds s^3 L_1^{3/2}\left(\frac{2\pi}{L_{max}}im'\right)F_{1m'}}^{b}. \tag{2.30}$$

Terms a and b in Eq. (2.30) are from the terms $|B|$ and $\partial_L q_{||}$ in the temperature evolution equation, Eq. (2.23), with the parallel heat flow defined in Eq. (2.24).

2.7.2 Speed dependence

The normalized speed dependence is also crucial in this research. We solve for F [Eq. (2.28)] on a grid in normalized speed, s. Since s is only a parameter in this equation, each processor can solve for F at independent values of s, which are determined by a numerical quadrature scheme used to compute the parallel heat flow:

$$q_{||} = -T\frac{4\pi}{3}v_T^4 \int_0^{\infty} ds s^3 L_1^{3/2}(s^2)\ F_1 \simeq -T\frac{4\pi}{3}v_T^4 \sum_{i=1}^{n_s} w_i s_i^3 L_1^{3/2}(s_i^2)\ F_1(s_i). \tag{2.31}$$

This approximation is a weighted sum of function values at n_s specified points (s_i) within the domain of integration.

2.7.3 Finite difference in time

A first-order finite-difference method is used to advance the system of equations in time until the steady state is reached. Approximating $\frac{\partial \mathbf{F}_{m'}}{\partial t}$ as $\frac{\mathbf{F}_{m'}^{k+1}-\mathbf{F}_{m'}^{k}}{\triangle t}$ we may rewrite Eq. (2.28) as

$$(\underline{\mathbf{I}}+\frac{\nu_L}{2}\triangle t\underline{\Gamma})\mathbf{F}_{m'}^{k+1} = -\mathbf{F}_{m'}^{k} - \triangle t\left[\left(\frac{2\pi}{L_{max}}im'\right)\underline{\mathbf{A}}v\mathbf{F}_{m'}^{k} + \underline{\mathbf{M}}v(\mathbf{F}^{k}B)_{m'}\right] + \left[\triangle t\ \delta_{l1}L_1^{\frac{3}{2}}v\left(\frac{2\pi}{L_{max}}im'\right)T_{m'}^{k+\frac{1}{2}}f_M - \delta_{l0}L_1^{\frac{1}{2}}(\partial_t T_{m'}^{k+\frac{1}{2}})f_M\right] \quad , \qquad (2.32)$$

and Eq. (2.30) as

$$T_{m'}^{k+\frac{3}{2}} = -T_{m'}^{k+\frac{1}{2}} - \triangle t\frac{8\pi}{9}v_T T_0\int dss^3 L_1^{3/2}(F_1^k B)_{m'} + \triangle t\frac{2}{3nT_0}S_{m'} + \triangle t\frac{8\pi}{9}v_T T_0\int dss^3 L_1^{3/2}\left(\frac{2\pi}{L_{max}}im'\right)F_{1m'}^{k}. \qquad (2.33)$$

The right side of the Eq. (2.32) is divided by the diagonal term on the left in order to provide some implicit stabilization and thus allow the system to reach steady state faster numerically. In addition, Eqs. (2.32) and (2.33) are staggered in time to allow for larger time steps. Staggering in numerical methods generally enhances accuracy and stability. Time staggering in our research means approximating F and T at interlaced time levels, one after the other.

In Eqs. (2.32) and (2.33) we choose integer levels t_k for $\mathbf{F}_{m'}$ and half-integer levels $t_{k+\frac{1}{2}}$ for $T_{m'}$. Level t_k denotes time, $t_k = k\triangle t$, with constant step size, $\triangle t$. This method thus steps from ($F_{m'}^{k}$, $T_{m'}^{k+\frac{1}{2}}$) to ($F_{m'}^{k+1}$, $T_{m'}^{k+\frac{3}{2}}$) with step size $\triangle t$. The initial value $T_{m'}^{\frac{1}{2}}$ is provided by the background temperature, T_0.

CHAPTER 3

RESULTS WITHOUT $|B|$ WELLS

In this chapter we present a computational investigation of heat flow transport in magnetized plasmas for different collisionality regimes. This chapter is divided into two parts. The first part, sections 3.1-3.2, presents convergence tests of the standard deviation in temperature as we refine our velocity space grid by increasing the number of Legendre polynomials and the number of speed points for different collisionality regimes. The goal of a convergence study is to minimize error and get an idea of how much resolution is needed to obtain a reliable numerical solution. The second part, sections 3.3-3.4, reports on the parallel electron heat flow in different collisionality regimes. Chapter 4 has similar studies, as in the second part of this chapter, but with the presence of the $|B|$ term in the F and T equations. All of the following studies are done assuming the plasma is in the steady state with heat flow parallel to the magnetic field balancing the static heat source.

3.1 Convergence of the Legendre polynomial expansion

The number of terms in the expansion of the distribution function [Eq. (2.18)] required to obtain convergent results depends on the number of Legendre polynomials, N. In practical calculations, one has to use a truncated expansion with a finite N. In this section we investigate the convergence of the Legendre polynomial expansion by computing the convergence of the standard deviation in temperature, σ_T, as Legendre polynomials are added to the expansion of the distribution function.

The standard deviation in temperature is defined as

$$\sigma_T = \sqrt{\frac{1}{n}\sum_{i=1}^{n}(T_i - \frac{1}{n}\sum_{i=1}^{n}T_i)^2} \quad , \tag{3.1}$$

where T is the dedimensionalized temperature and $n = 100$ uniformaly spaced points in the domain. Fig. 3.1 shows the convergence of σ_T as Legendre polynomials are added to

the expansion for a nearly collisionless case with the ratio of collision length, L_v, to source gradient scale length, L_s, of $L_v/L_s = 10$. The number of Legendre polynomials required to obtain converged results in this regime where collisions are infrequent is around $N = 16$.

In the limit where collisions dominate (small collision length $L_v/L_s \ll 1$), convergence is obtained even for as few as two Legendre polynomials, $N = 2$ (see Fig. 3.2). This agrees with previous work [10, 25, 26]. In the collisional limit, collisions easily destroy the details in the pitch-angle direction of velocity space, but in the nearly collisionless limit, more Legendre polynomials are required to obtain a converged solution.

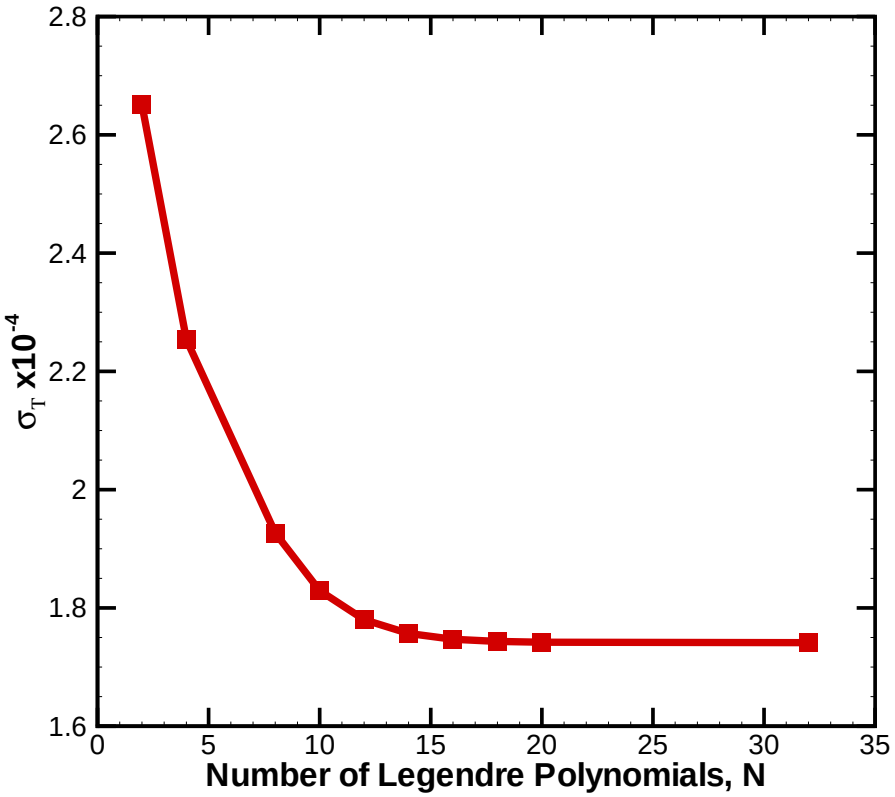


FIG. 3.1. Plot shows convergence of the standard deviation in temperature, σ_T, in the nearly collisionless limit as Legendre polynomials are added to the expansion. Convergence in this limit with $L_v/L_s = 10$ requires $N = 16$.

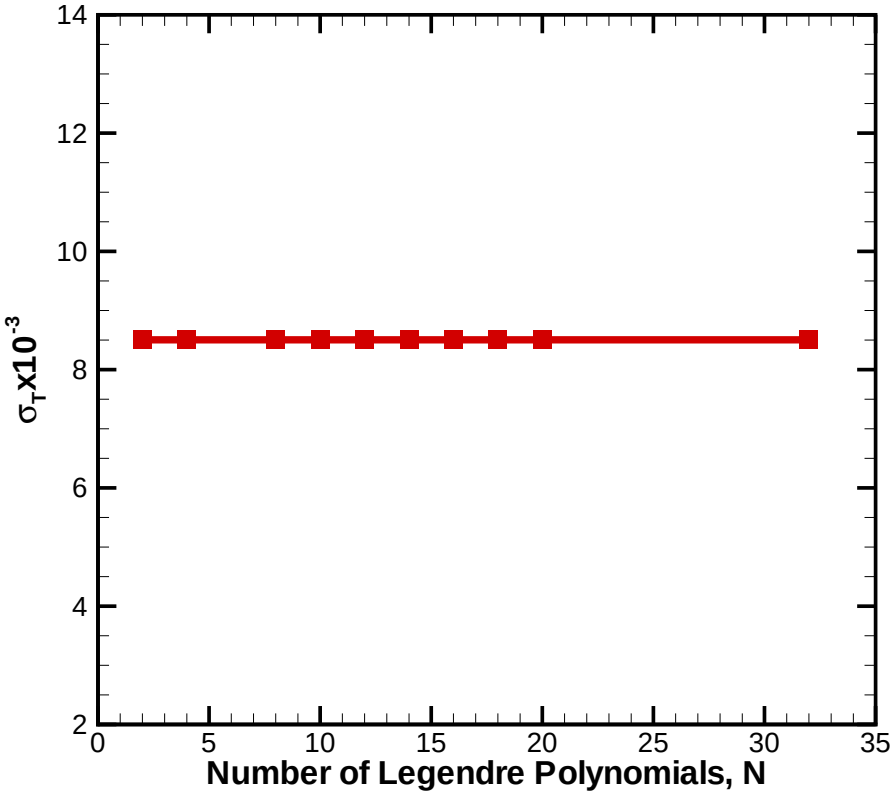


FIG. 3.2. Convergence of the standard deviation in temperature, σ_T, in the collisional limit as Legendre polynomials are added to the expansion. Convergence in this limit is rapidly obtained and requires only N=2. Here $L_v/L_s = 10^{-3}$ and the results for $N = 2$ and higher are identical.

To determine how large the error is in the variance of temperature, we define the relative error as

$$\varepsilon_{\sigma T} \equiv \frac{|\sigma_T - \sigma_{T(exact)}|}{|\sigma_{T(exact)}|}, \tag{3.2}$$

where $\sigma_{T(exact)}$ is the standard deviation in temperature for the highest number of Legendre polynomials, i.e., our most refined case.

In the collisional regime, σ_T was converged for only $N = 2$ Legendre polynomials, so we are interested only in the low-collisionality regime to find the relative error. Fig. (3.3) reveals spectral convergence with the relative error of the standard deviation in temperature, ε_{σ_T}, decreasing exponentially with increasing number of Legendre polynomials. In the collisionless regime, the $N = 16$ case has an error roughly two orders of magnitude smaller than the $N = 2$ case.

As mentioned previously, convergence occurs more quickly as the collision frequency increases. This is expected since weak collisionality is associated with fine-scale structures in pitch angle, $v_{||}/v$. At very low values of the collision frequency, the structure in $v_{||}/v$ becomes more complex, thus requiring more Legendre polynomials.

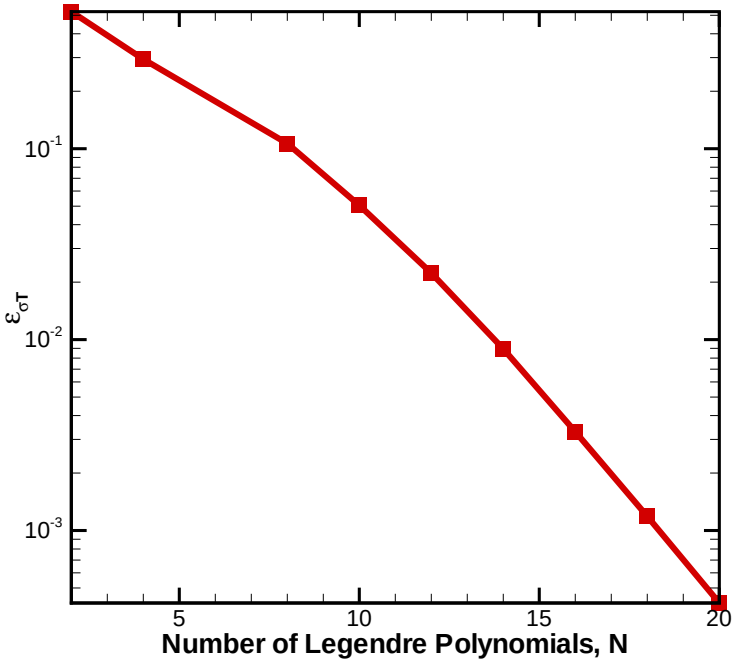


FIG. 3.3. Relative error, ε_{σ_T}, of the standard deviation in temperature, defined in Eq. (3.2) in the nearly collisionless limit. Plot shows spectral convergence with the error decreasing exponentially with increasing N.

3.2 Convergence of the speed representation

As a further test to determine whether velocity space is well-resolved, we check for convergence in our speed representation by adding grid points until quantities of interest are unchanged. Again this test involves computing the standard deviation in temperature for different collisionality. Because this process can be computationally time consuming, we do parallel computations on a multiprocessor system by assigning each processor a speed grid point, $s = v/v_T$.

In this section, we evaluate the number of speed points, n_s, required to obtain converged results in the collisional and nearly collisionless regimes. As mentioned above, processors can solve for the distribution function at their s values independent of the other processors. They must communicate, however, in order to compute the parallel heat flow moment, which is needed to advance temperature. Here all the results are obtained by keeping the number of Legendre polynomials at $N = 16$.

As a reminder, the parallel heat flow moment can be written as

$$q_{||} = -T \int d\mathbf{v} v_{||} L_1^{3/2} \sum_n F_n P_n \left(\frac{v_{||}}{v}\right) = -\frac{4\pi}{3} v_T^4 T \int_0^\infty ds s^3 L_1^{3/2}(s^2) F_1(s,L,t)$$
$$\simeq \frac{4\pi}{3} v_T^4 T \sum_{i=1}^{n_s} w_i s_i^3 L_1^{\frac{3}{2}}(s_i^2) F_1(s_i,L,t), \qquad (3.3)$$

where w_i and s_i are the weights and nodes of an n_s point Gaussian quadrature scheme. Each processor solves for one coefficient $F_1(s_i,L,t)$ needed to compute $q_{||}$. Such problems in parallel computing where the communication time is miniscule compared to the independent processor computation time are referred to as embarrassingly parallel. This behavior makes convergence test in speed relatively quick and easy.

3.2.1 Speed convergence in the collisional regime

Fig. 3.4 shows the convergence of the standard deviation in temperature defined in Eq. (3.1), as more speed points are included in the velocity grid for the collisional regime, $L_v/L_s = 10^{-3}$. In this case the background temperature, $T_0 = 10eV$, and the corresponding thermal speed is $v_T = 1.8 \times 10^6 m/s$. In this short mean-free path regime, although high-energy electrons are responsible for carrying the heat flow [27], convergence is rapidly achieved with $n_s = 4$. In terms of Gaussian quadrature, which is exact for integrands that are polynomials of order $2n_s - 1$ or less, this implies the F_1 coefficient in the Legendre expansion for the distribution function is well approximated by a relatively low-order polynomial in s.

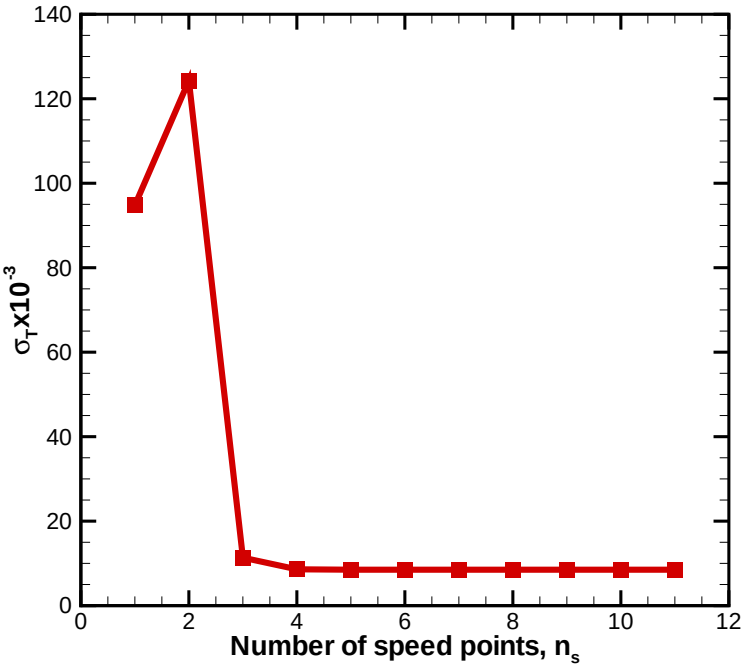


FIG. 3.4. Convergence of the standard deviation in temperature, σ_T, in the collisional limit as speed points are added to the expansion. Convergence in this limit, $L_v/L_s = 10^{-3}$ requires $n_s = 4$.

The relative error in σ_T for the collisional limit is shown in Fig. 3.5. In this short mean-free path case, collisions again smooth out details in velocity space and aid rapid convergence. There are approximately three orders of magnitude reduction in the error between the $n_s = 2$ and $n_s = 4$ cases.

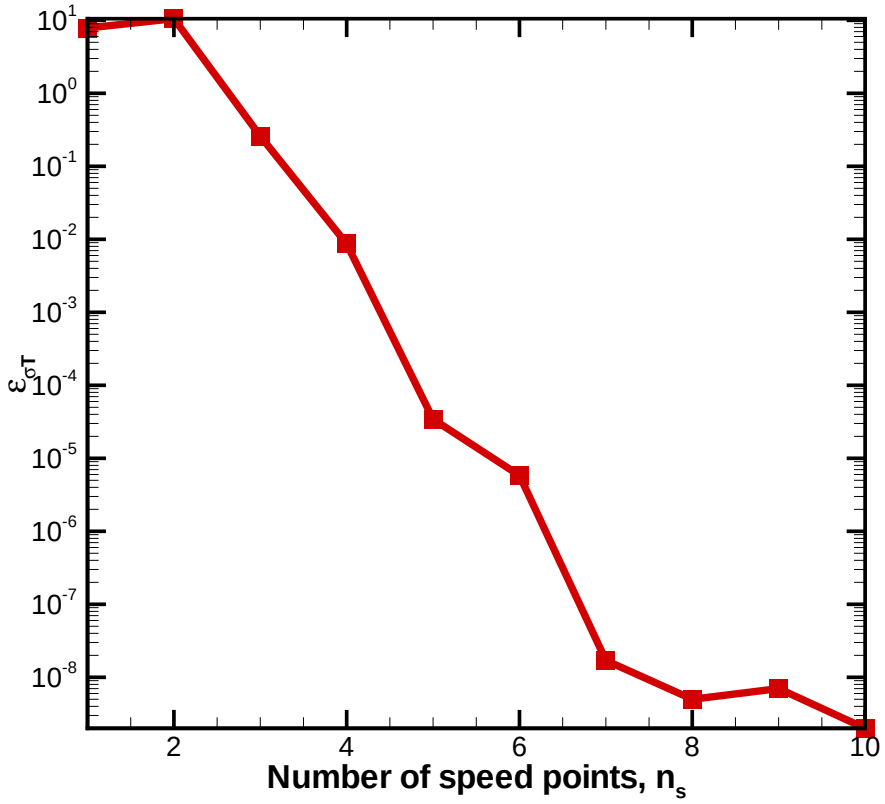


FIG. 3.5. Relative error, ε_{σ_T}, of the standard deviation in temperature defined in Eq. (3.2) as a function of the number of speed grid points, n_s. The error falls rapidly with increasing n_s in the collisional regime.

3.2.2 Speed convergence in the nearly collisionless regime

In the regime where collisions are infrequent, it becomes more difficult to show uniform convergence as n_s is increased. Compared to the collisional and moderately collisional

regimes, the high temperature in nearly collisionless regimes also delays achieving the steady state, thus making these convergence tests more costly computationally. Fig. 3.6 shows the convergence of σ_T when the background temperature is high, $T_0 = 1KeV$. At such a high temperature, convergence of σ_T is difficult to obtain. A possible improvement may be to adjust the number of Legendre polynomials, N, and n_s simultaneously so velocity space refinement happens uniformly in two dimensions. Here we have fixed N at 16. In this regime, the heat is carried by the thermal electrons.

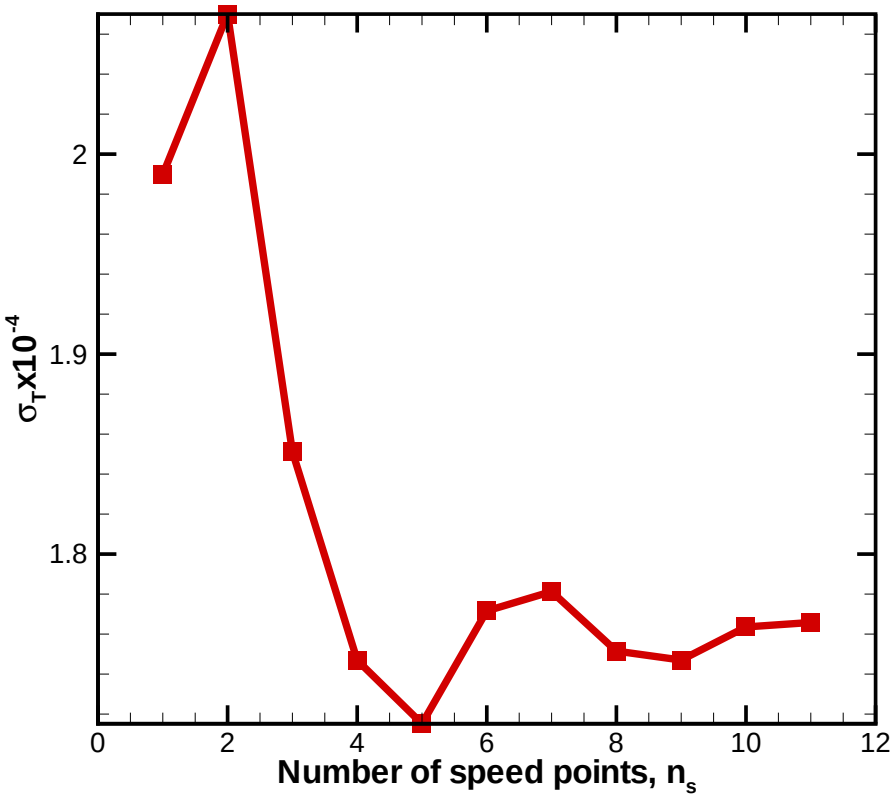


FIG. 3.6. Check for the convergence of the standard deviation in temperature, σ_T, in the nearly collisionless regime as speed points are added to the expansion. Convergence in this limit is harder to obtain.

Compared to the value of σ_T in collisional regime, see Fig. 3.2 where $\sigma \approx 10^{-3}$, the standard deviation in temperature for this regime is much smaller in value. This arises from the fact parallel heat transport is more robust in high-temperature plasmas, and hence the perturbations/fluctuations in T are smaller. As we add more speed points to the grid, σ_T tends towards a converged value. However, it is hard to maintain steady state at such high temperatures, therefore complete convergence of σ_T in this regime is also hard to achieve.

Fig. 3.7 shows the relative error in σ_T for the nearly collisionless limit. Compared to the collisional regime, the relative error is not a smooth curve; and it shows some fluctuations with increasing number of speed points.

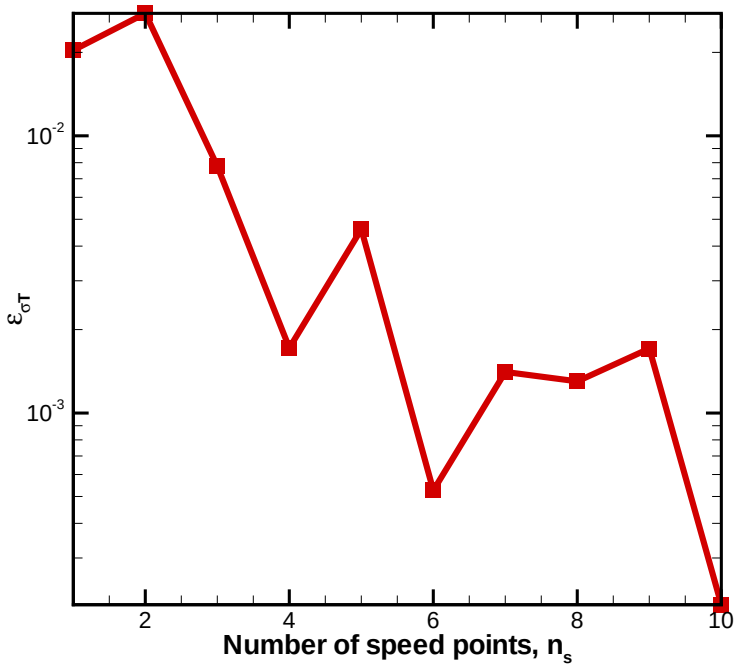


FIG. 3.7. Relative error, ε_{σ_T}, of the standard deviation in temperature in the nearly collisionless regime. In order to achieve a uniform convergence it may be necessary to refine our velocity space representation in two dimensions simultaneously or include speed diffusion and drag effects in our collision operator.

As suggested earlier, it may be necessary to refine velocity space representation for F in $v_{||}/v$ and s simultaneously in order to see more uniform convergence in these nearly collisionless cases. Another area of improvement would be to use a more accurate collision operator that includes speed diffusion and drag effects. This could smooth out details in the speed direction in the same way the Lorentz pitch angle scattering operator smooths out the distribution function in $v_{||}/v$.

3.3 Heat flow in different collisionality regimes without magnetic wells

One main motivation for this work was to discover how the physics of parallel electron heat flow changes for various collisionality regimes. In order to simplify the problem, we have solved the equation for the distribution function, Eq. (2.22), along with the temperature equation, Eq. (2.23), without $|B|$ effects, that is, without magnetic wells, which complicate the heat transport by trapping electrons locally in our 1-D spatial domain. The effects of magnetic wells will be discussed in Chapter 4.

3.3.1 Temperature-dependent heat flow

In a collision-dominated plasma, parallel heat flow is driven by local parallel gradients in temperature. In this limit, the general, nonlocal heat flow closure reduces to the diffusive form, which defines the parallel heat-flow at any point in the plasma as being proportinal to the minus local parallel temperature gradient, that is, $q_{||} \sim -\nabla_{||}T$. This behavior can be seen in Fig. 3.8 where the solid curve represents normalized steady-state temperature for a heat source, $S = S_0 cos\left(\frac{2\pi L}{L_s}\right)$, with the heat source scale length, $L_s = 100m$. Regions of higher (lower) temperature are where the plasma is being heated (cooled) and the heat flow, $q_{||} \sim -\nabla_{||}T$, maintains the steady state. The heat flow is given by the dashed curve in Fig. 3.8. The direction of heat flow in the collisional regime is down the temperature gradient.

In moderate-space and low-collisionality regimes, the gradient in temperature again plays an important role in determining the parallel heat flow. In these regimes, the heat

flow and the temperature profile look similar to that shown in Fig. 3.8, but the fluctuation in the temperature, δT, is smaller compared to the collisional case. This result is shown in Fig. 3.9 where the solid curve represents the normalized steady state T for the moderate collisionality regime ($T_0 = 100eV$) and the dashed-dot curve represents the normalized T for the nearly collisionless regime ($T_0 = 1KeV$). Comparision of Figs. 3.8 and 3.9 reveals with decreasing collision frequency, the variance of temperature decreases. This is due to the fact more energetic electrons are able to smooth out temperature perturbations along field lines in higher-temperature plasmas.

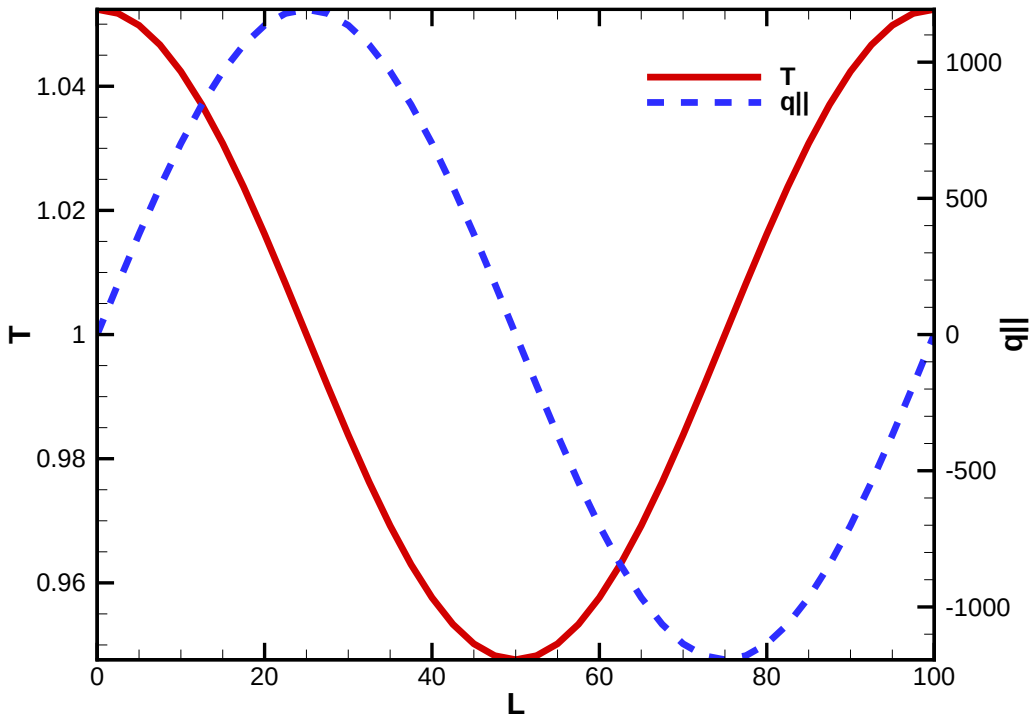


FIG. 3.8. Variation in normalized parallel electron heat flow and the normalized steady-state temperature. For this collisional regime the background temperature $T_0 = 10$eV. Parallel heat flow is proportional to the parallel temperature gradient. Here the $|\mathbf{B}|$ term is not used in the equations.

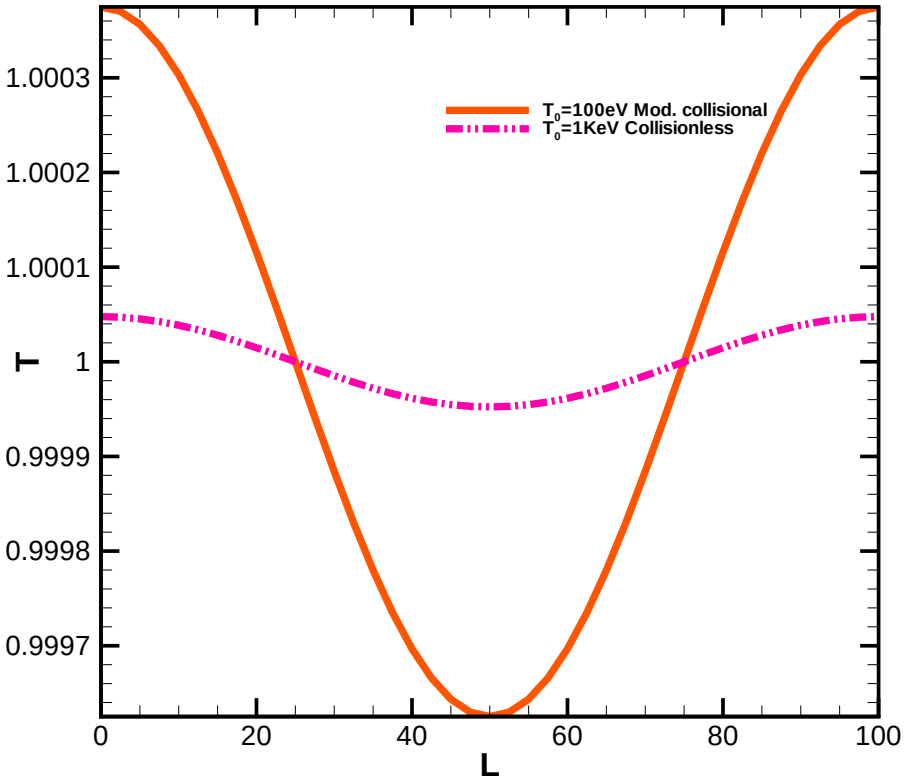


FIG. 3.9. This plot for higher-temperature, lower-collisionality regimes looks similar to the one for higher collisionality, but with a smaller fluctuation in temperature.

3.3.2 σ_T decreases with decreasing collisionality

At low temperatures and high densities, plasmas are collisional. In the collisional regime heat flow is diffusive in nature. At higher temperatures, the plasma becomes less collisional and the free streaming of the electrons dominates the heat flow. As the background temperature increases from 10 eV to 1000 eV, the variance in temperature decreases due to more energetic electrons carrying heat more effectively along field lines.

In Fig. 3.10, the ratio of collision length, $L_\nu \equiv \frac{v_T}{\nu_L}$ [ν_L is defined in Eq. (2.6)], to source scale length, L_ν/L_s defines the collisionality. In high collisionality regimes, collision length

is very small compared to the source scale length and particles collide more frequently leading to diffusive transport and larger variations in temperature. As the collision length increases with increasing background temperature, collisions become less frequent and the variation in temperature decreases.

3.4 Distribution function in different collisionality regimes

In this section, the computational results are presented in the form of contour plots of the distribution function in various collisionality regimes without $|\mathbf{B}|$ effects. All results here were obtained keeping the number of Legendre polynomials $N = 16$ and the number of speed points $n_s = 5$.

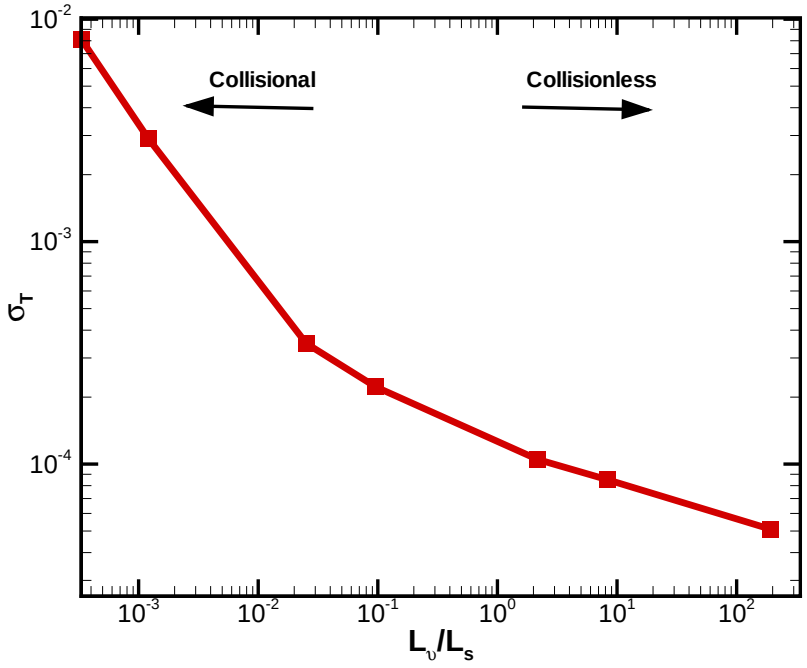


FIG. 3.10. This plot shows the standard deviation in temperature, σ_T, as collisionality varies. σ_T decreases for less collisional regimes as hotter electrons more efficiently smooth out perturbations in T along field lines. However, this effect seems to weaken as we move to the nearly collisionless regime, something referred to as flux-limited transport.

3.4.1 Collisional regime

Fig. 3.11 shows the distribution function, F, in the collision dominated regime, $L_\nu/L_s < 10^{-3}$. The evolution equation for F involves four independent variables, $\frac{v_{||}}{v}$, s, L, and t. We plot F in the steady state at the speed grid point $s = 5$. Along the vertical axis $\frac{v_{||}}{v}$ takes on the value $+1$ (-1) for electrons traveling parallel (anti-parallel) to the magnetic field and 0 for electrons whose motion is purely devoted to gyration about $\mathbf{B}$. The horizontal axis is our 1-D domain in space, $X\varepsilon[0,1]$ where $X \equiv L/L_{max}$.

In the collisional steady state with $\mathbf{v}\cdot\nabla F$ small, the Lorentz operator may be trivially inverted. The thermodynamic drive of interest is from the $n = 1$ term on the right side of Eq. (2.22) and we have

$$F_1 \simeq \frac{2}{\nu_L} v_T s L_1^{\frac{3}{2}} \partial_L T \frac{f_M}{T_0}. \tag{3.4}$$

Consistent with Eq. (3.4), Fig. 3.11 shows the distribution function, F, vanishes where the gradient in temperature is 0 and is maximum where the gradient in temperature is maximum. The symmetery in F also reveals in the high-collisionality regime, there are equal number of particles moving in opposite directions at a given time carrying heat past a local point in a diffusive fashion. This is the up-down asymmetry in $v_{||}/v$ shown in the contours of Fig. 3.11.

3.4.2 Moderate collisionality regime

Between the collisional and collisionless limits, there exists a wide range of intermediate collisionality relevant to fusion plasmas and many other applications. The regime of intermediate collisionality, which is studied in this section, is between the long wavelength classical Braginskii limit and the short wavelength regime of weak collisions. Fig. 3.12 shows contours of F at $s = 5$ for the moderatly collisional regime between $10^{-3} < L_\nu/L_S < 10^1$.

Compared to Fig. 3.11 for the collision dominated regime, contours of the distribution function are slanted and suggest a nonlocal aspect to the transport. The tilt suggests the particles carrying heat in opposite directions at a given time past a local point are not exactly opposite to each other in velocity space. That is there is an asymmetery in the distribution of the particles due to the nonlocal behavior of the transport which cannot be accounted for in the local, collisional expression given in Eq. (3.4).

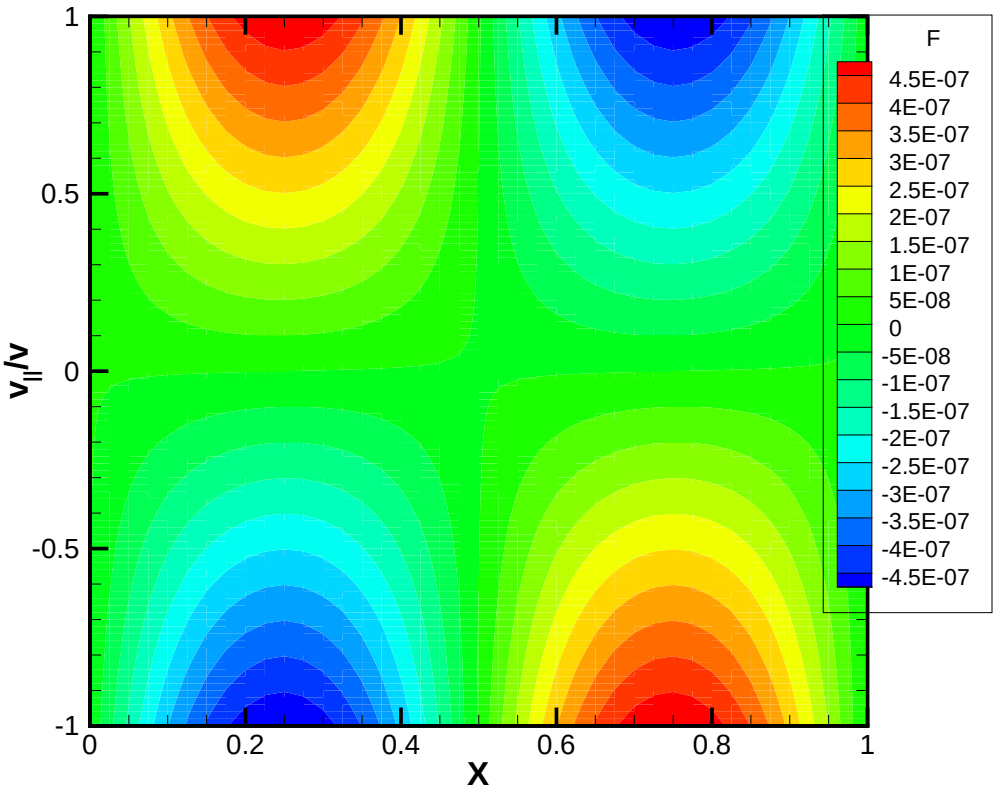


FIG. 3.11. Contours of the distribution function at $s = 5$ in the collisionl regime with $L_v/L_s = 10^{-3}$. The variation in $X = L/L_{max}$ is due to the sinusoidally varying heat source. The up-down asymmetry in $v_{||}/v$ indicates the local diffusive nature of transport down the local T gradient.

3.4.3 Nearly collisionless regime

Fig. 3.13 shows the contours of the distribution function in the high-temperature regime with $L_v/L_s \geq 10^1$. Here the tilted nature of the contours is even more evident than in the intermediate-collisionality regime. The contours suggest the nonlocal effects are critical in this regime. In the absence of collisions, the particles move freely along field lines and the distribution of particles in velocity space can develop small scales in velocity space [28]. Note the distribution function does not vanish in the region where the gradient in temperature is 0, that is $F \neq 0$ even where $\partial_L T = 0$, hence in the steady-state this effect must be due to the advective term in our kinetic equation. Also, electrons with small $v_{||}/v$ seem to be responsible for the transport. This makes sense if we consider them moving slowly along field lines between regions of different T and hence, having time to irreversibly deliver heat via collisions.

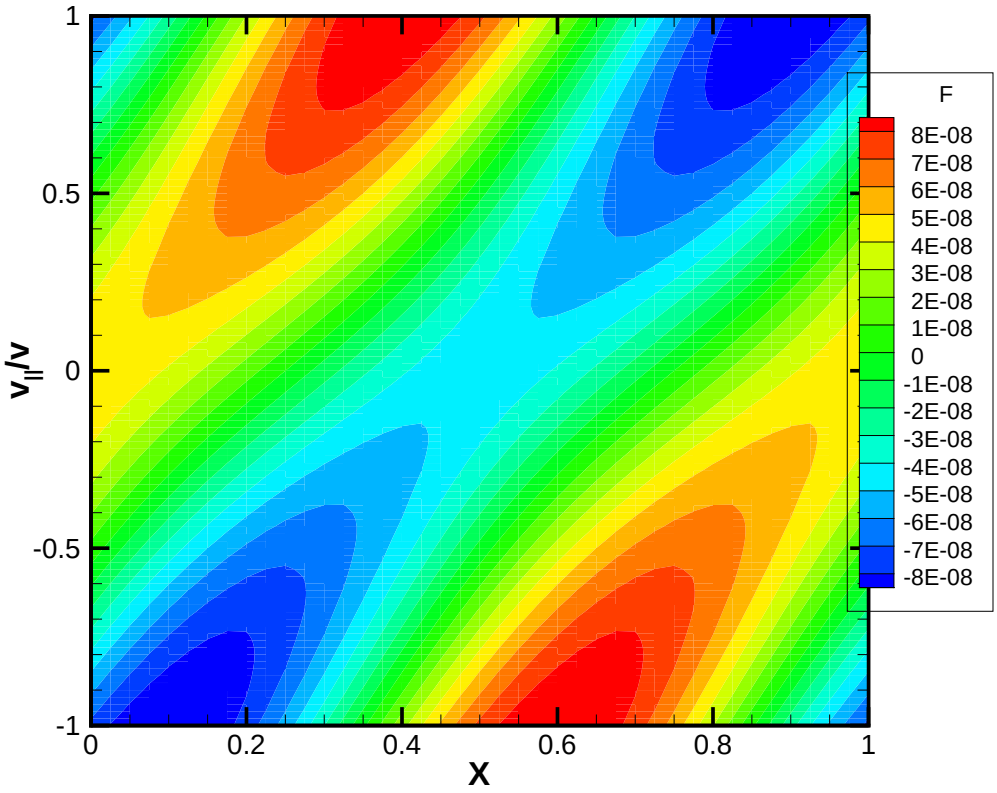


FIG. 3.12. Contours of the distribution function at $s = 5$, in the regime of intermediate collisionality with $L_v/L_s = 10^{-2}$. Here we interpret the displaced asymmetry in $v_{||}/v$ as an indication of nondiffusive, nonlocal transport arising from the $\mathbf{v}_{||} \cdot \nabla F$ term in our kinetic equation.

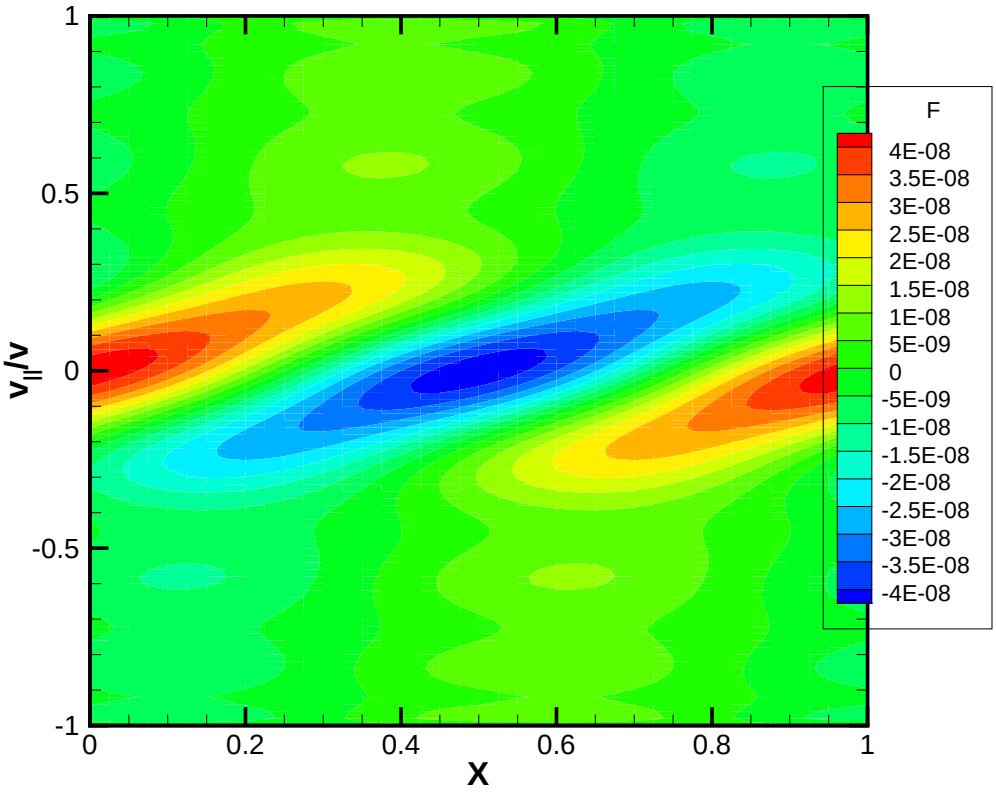


FIG. 3.13. Contours of the distribution function in the nearly collisionless regime with $L_v/L_s = 10$. Evidence of nonlocality is apparent in the fact that F does not vanish where the temperature gradient is zero near $X = 0, 0.5$ and 0.1.

CHAPTER 4

RESULTS WITH MAGNETIC WELLS

This dissertation focuses on the effect of an inhomogeneous magnetic field on parallel electron heat flow and temperature equilibration along magnetic field lines. In this chapter, the parallel electron heat flow in an inhomogeneous magnetic field is calculated for arbitrary collisionality and compared to the results without magnetic wells presented in Chapter 3. In order to quantify heat transport, we again compute the standard deviation in the steady-state temperature with the term $\partial_L lnB$ acting in the F and T equations, Eqs. (2.22) and (2.23), respectively. Section 4 reports on the steady-state temperature distribution along field lines in different collisionality regimes as we vary the magnetic well depth. The results are obtained using the convergent values obtained in the first part of Chapter 3 with the number of Legendre polynomials, $N = 16$, and the number of speed points, $n_s = 5$.

The term representing magnetic wells in the F and T equations is of much importance in this work due to the fact variations in magnetic field strength lead to a population of trapped particles in velocity space and have a squeezing effect on the heat flow. The sinusoidal magnetic wells are defined as

$$B(L) \quad = \quad B_0 + B_c \, cos(\frac{2\pi L}{L_B}). \tag{4.1}$$

Using the above definition of magnetic wells, the $\partial_L lnB$ term referred to as mod-B ($|\mathbf{B}|$) in our F and T equations becomes

$$\partial_L lnB = \frac{1}{B(L)}\partial_L B \simeq \frac{1}{B_0}\partial_L B = -\frac{B_c}{B_0}\left(\frac{2\pi}{L_B}\right) sin\left(\frac{2\pi L}{L_B}\right). \tag{4.2}$$

Here L_B is the magnetic field scale length. We define the magnetic well depth as $\delta B = B_c/B_0$ and from now onwards will refer to the approximation in Eq. (4.2) as a linear mod-B case, since it uses B_0 as opposed to $B(L)$ in the denominator. The phenomenon of trapping

may be illustrated by considering a particle's pitch angle when it is at the minimum in the magnetic field ($L = nL_B/2$) where

$$\frac{v_{||}}{v}\left(\frac{L_B}{2}\right) = \pm\sqrt{1-\frac{\mu B_{min}}{w}}, \tag{4.3}$$

and n ranges from 1 to the number of magnetic wells in our domain. Here $\mu = \frac{1}{2}mv_{\perp}^2/B(L)$ is the approximately conserved magnetic moment, $w = \frac{1}{2}mv^2$ is the approximately conserved kinetic energy and $B_{min} = B_0 - B_c$. As they travel away from a minimum in B, particles with constant $\frac{\mu}{w} = \frac{1}{B(L)}$ for $L\varepsilon[0, L_{max}]$ will have $v_{||}/v$ go to zero and be reflected. This is what it means to be trapped.

A spatially varying heat source, S, is turned on and the temperature in the system starts evolving with time. Fig. 4.1 shows the variation of S (dashed curve) and $B(L)$ (solid curve), defined in Eq. (4.1), with a source scale length, $L_s = 100m$, in the moderate collisionality regime, $\frac{L_v}{L_s} = 10^{-1}$. Here the heat source is defined as

$$S = S_0\, cos\left(\frac{2\pi L}{L_s}\right). \tag{4.4}$$

For this case $\delta B = 0.2$, the source strength, $S_0 = 50$, and again the sinusoidally varying heat source satisfies $\int_0^{L_{max}} dL\, S = 0$. The source strength is kept the same for all the results obtained in the following sections.

4.1 $q_{||}$ in the presence of magnetic wells for various collisonality regimes

In this work, it is shown the steady-state temperature variations along magnetic field lines in an inhomogeneous magnetic field are enhanced by the presence of magnetic wells. In lower collisionality regimes, this may be attributed to the fact the trapped population does not contribute to heat flow over gradient scale lengths in temperature longer than mod-B well lengths. Compared to the previous theory, where L_B was ordered small compared to the temperature gradient scale length, $L_T = (\partial_L lnT)^{-1}$, in this work the ordering of L_B is

independent of L_T (or L_s), thus making the results more general.

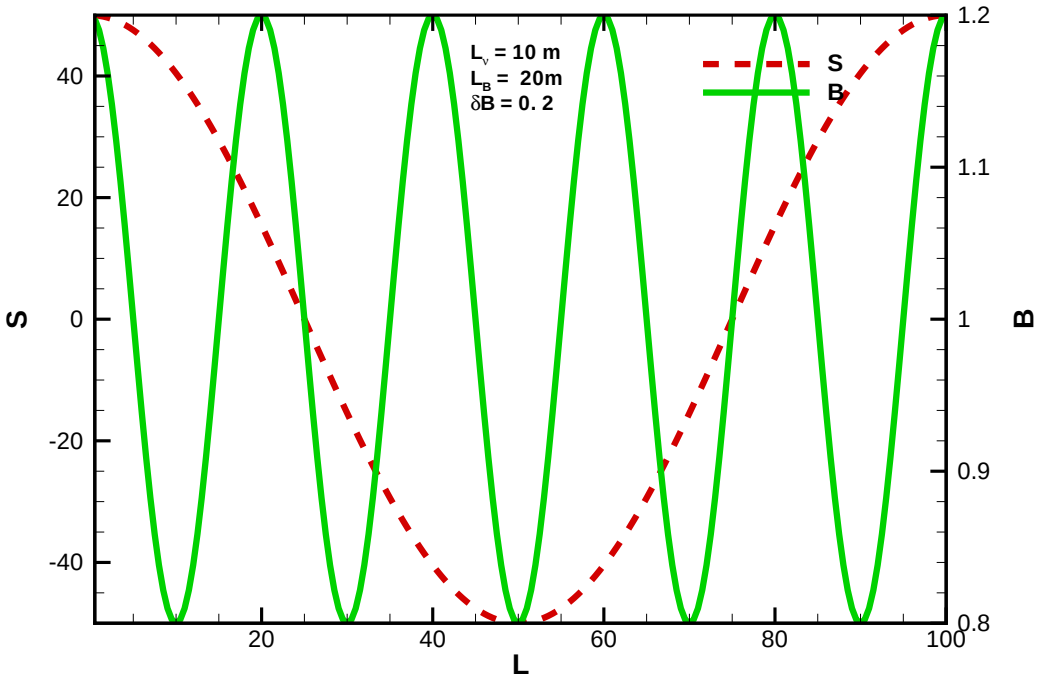


FIG. 4.1. Plot shows variation in B and the spatially varying heat source, S, with a scale length of 100m. The magnetic well scale length $L_B = 20$m. For this moderately collisional plasma, $L_\nu/L_s = 10^{-1}$ and the well depth is $\delta B = 0.2$.

4.1.1 Temperature in the presence of magnetic wells

In a typical magnetized laboratory plasma, such as tokamaks, temperature can be a very complicated function of distance along the magnetic field line. Fig. 4.2 shows the variation in normalized temperature in the presence of magnetic wells with varying well depths. The dashed-dot curve shows the variation in normalized T in the absence of $|\mathbf{B}|$ effects. This curve is similar to the dashed-dot curve in Fig. 3.9 for the moderate collisionality regime with $L_\nu/L_s = 10^{-1}$. The dashed curve and the solid curve represent the variation in T for magnetic well depth 0.2 and 0.4, respectively. The dotted curve shows mod-B as a function of L. The source and gradient in magnetic field is same as shown in Fig. 4.1 and L_B is

comparable to the collision length, $L_\nu = 10m$, an ordering that is not possible in bounce-averaged theories [11]. In this regime the presence of magnetic wells fundamentally alters the temperature distribution along magnetic field lines.

In the absence of the magnetic wells, the fluctuations in temperature are more effectively smoothed out because all electrons are passing and can carry heat along the field line. With the presence of magnetic wells, particles get trapped and are unable to carry heat over longer-scale lengths. This leads to larger temperature fluctuations. As we increase the well depth, more and more particles get trapped and local perturbations in the temperature are visible. From the curve with $\delta B = 0.4$, it seems the temperature profile has features that are tied to the minima and maxima in B.

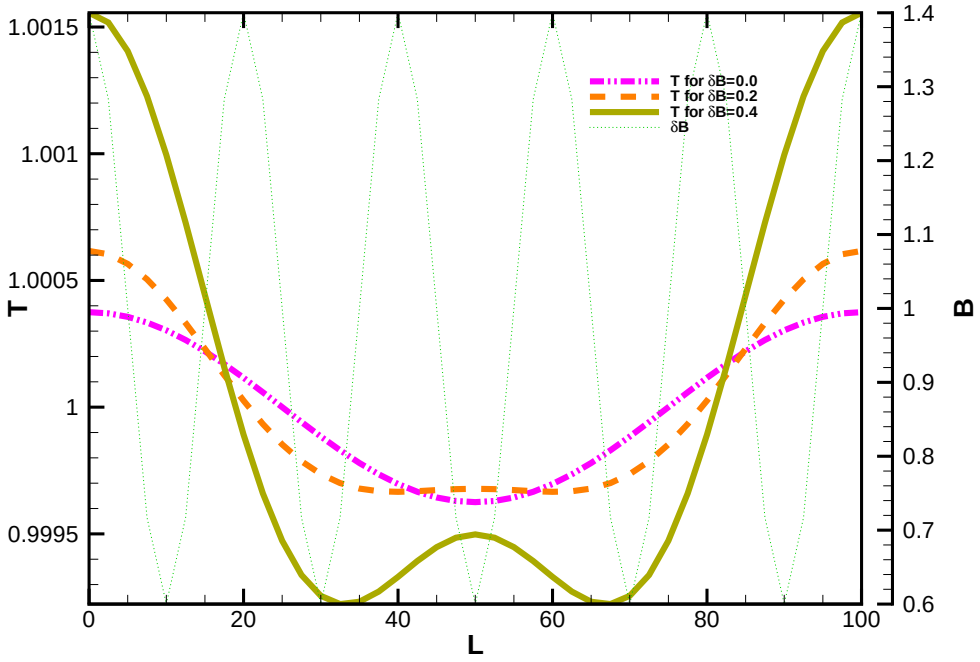


FIG. 4.2. This plot shows the effect of the $\partial_L lnB$ term on temperature in the moderately collisional regime. The magnetic well depths are δB =0.0, 0.2 and 0.4. The variance in temperature increases as the magnetic well depth increases.

4.1.2 σ_T increases with increasing well depth

As shown in Fig. 4.2, with increasing magnetic well depth the variance in temperature increases and some distortion in the temperature profile occurs due to $|\mathbf{B}|$ effects. The local effect of $\partial_L lnB$ determines the form for the temperature distribution along the field line based on collisionality and trapped/passing effects. With increasing δB, more and more particles get trapped in magnetic wells.

It can be observed from Fig. 4.3 that, in the collisional regime, the increase in σ_T with increasing δB is purely a fluid effect. This case corresponds to the collisional result A as shown in Fig. 4.5 for $\delta B = 0.4$. The red dashed curve in Fig. 4.3 is obtained by considering the presence of the $|\mathbf{B}|$ term only in the temperature evolution equation. This corresponds to adding the $q_{||}\partial_L lnB$ term in the T equation, which has a squeezing effect on the heat flow, but not including the $\partial_L lnB$ term in our kinetic equation. With the $|\mathbf{B}|$ term in the F equation, as well (green dash-dot curve) we see little change in σ_T from the previous case. This implies trapped particles do not contribute to the transport. Here trapped is a misnomer since collisional particles are unable to execute bounce orbits. In the collisional regime, particles undergo frequent collisions and the transport is predominantly diffusive.

To obtain these results, the depth of the wells is taken only up to $\delta B = 0.4$, since further increasing the well depth causes a sudden increase in σ_T. The sudden increase in σ_T is partially due to the fact that in obtaining the following results, we treated $\partial_L lnB$ linearly. The difference here between linear versus nonlinear is we used the constant B_0 instead of the full $B(L)$ in the denominator of Eq. (4.2). It can also be observed from Fig. 4.3 there is a slight effect of the $|\mathbf{B}|$ term in the F equation for well depth in the range $0.1 < \delta B < 0.3$.

The δB scan in Fig. 4.4 is done in the moderately collisional to nearly collisionless regime, point B in Fig. 4.5. In this case, the $|\mathbf{B}|$ term reduces heat flow parallel to magnetic field due to more particles getting trapped in the wells. This in turn causes more variance in temperature. When the $|\mathbf{B}|$ term is not used in the F equation, then the heat flow is mainly

due to particles free streaming along the magnetic field lines. Here also the dashed red curve in Fig. 4.4 shows the standard deviation in temperature when the $|\mathbf{B}|$ term is not used in the F equation and is present only in the T equation.

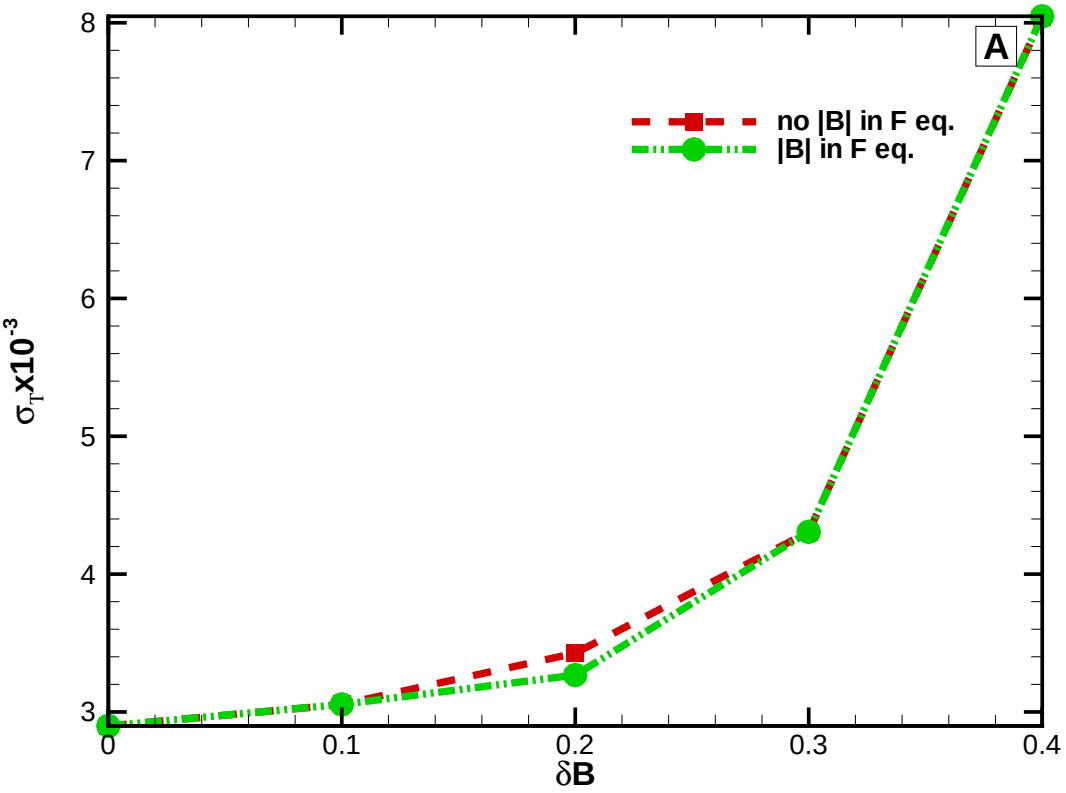


FIG. 4.3. The standard deviation in temperature, σ_T, versus change in magnetic well depth, δB, is plotted. This scan was done for the collisional case shown as A in Figure (4.5). The fact that there is little difference between the cases with and without $|\mathbf{B}|$ in our kinetic equation indicates that the transport is diffusive.

In the moderately collisional to collisionless regime, increasing magnetic well depth again increases the standard deviation in temperature. Additionally, the presence of $|\mathbf{B}|$ in our kinetic equation also increases σ_T unlike in the collisional regime where the $|\mathbf{B}|$-in-F and no-$|\mathbf{B}|$-in-F cases were similar. We attribute the increase in σ_T when going from the no-$|\mathbf{B}|$-in-F case to the $|\mathbf{B}|$-in-F case to the purely kinetic effect of particle trapping.

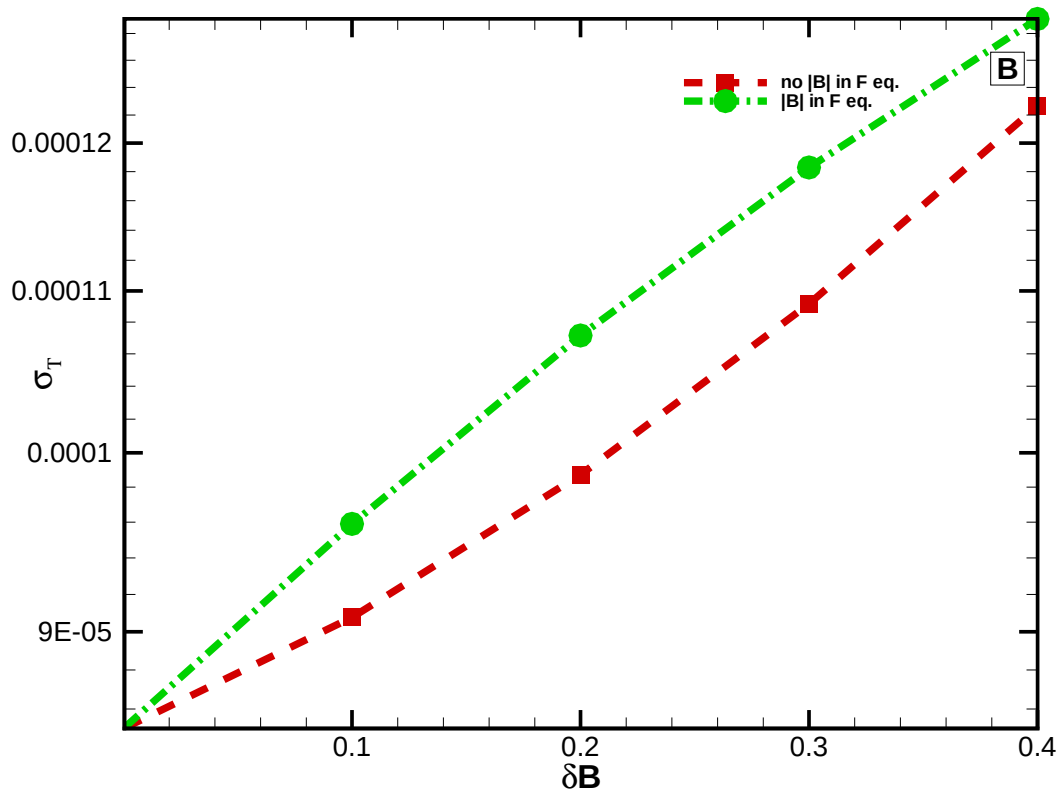


FIG. 4.4. The standard deviation in temperature, σ_T, versus change in magnetic well depth, δB, is plotted. Point B here corresponds to the point B in Figure 4.5. The entire scan is done in the moderately collisional to collisionless regime. The dashed red curve shows the standard deviation in temperature when $|\mathbf{B}|$ is not used in the F equation, but is present only in the T equation. The green curve is the true result indicating particle trapping reduces heat flow parallel to the magnetic field.

4.1.3 Effect of $|\mathbf{B}|$ on the σ_T for different collisionality regimes

Fig. 4.5 shows the plot of σ_T for varying collisionality with and without the $|\mathbf{B}|$ effect. Here with $|\mathbf{B}|$ means the $|\mathbf{B}|$ terms are present in the F and T equations and without $|\mathbf{B}|$ means no magnetic wells, as presented in Chapter 3. It is observed irrespective of the presence of magnetic wells, the standard deviation in temperature decreases for less collisional

regimes because the fluctuations in temperature are more efficiently smoothed out by the hotter electrons responsible for heat flow parallel to the magnetic field. In the presence of magnetic wells, however, we see an increase in the fluctuation due to two effects: (i) the squeezing effect caused by the $q_{||}\partial_L lnB$ term in the T equation and (ii) the particle trapping effect due to $\mathbf{F}\partial_L lnB$ in the F equation. With $L_s = 100m$ and $L_B = 20m$, we estimate effect (i) is dominant for $L_\nu/L_s < 10^{-1}$ and effect (ii) becomes important for $L_\nu/L_s > 10^{-1}$.

The red dashed curve in Fig. 4.5 represents σ_T without the presence of magnetic wells and is the same as the red bold curve in Fig. 3.10. The green solid curve shows the effect of $|\mathbf{B}|$ on σ_T. Here points A and B corresponds to the points A and B in the collisional and low collisionality regimes shown in Figs. 4.3 and 4.4, respectively. The results in this figure are obtained for the well depth, $\delta B = 0.4$.

4.2 Distribution function in different collisionality regimes with $|B|$ effects

In the presence of magnetic wells, some electrons get trapped, while others are passing and contribute to the heat flow along the magnetic field lines. However, the contribution to temperature equilibration along magnetic field lines comes not only from the free streaming of untrapped electrons in the F equation, but also from the $\partial_L lnB$ term in the steady-state temperature equation, namely,

$$\partial_L q_{||} = S + q_{||}\partial_L lnB. \tag{4.5}$$

In the collisional regime with collision length L_ν=0.12 m, particles cannot execute bounce orbits and transport can be understood in terms of a simple diffusion process. Contours of the distribution function in steady state in this regime are plotted in Fig. 4.6 for $s = 5$. It is observed, for the most part, in this short mean-free path regime, F is not affected by the presence of magnetic wells and there are equal number of particles moving in opposite directions. Because collisions are frequent, particles cannot get trapped in the magnetic

wells. In the collisional regime, trapping applies only to high-energy (high s) electrons whose bounce frequency in magnetic wells is higher than their collision frequency. Although this is still possible in the collisional regime because of the $1/s^3$ dependence in the collision frequency and the s dependence in the bounce frequency, the only slight distortion in the contours suggests for $s = 5$, collisions are still dominant. We have chosen the well depth, $\delta B = 0.4$ in this case, which corresponds to point A in Fig. 4.3.

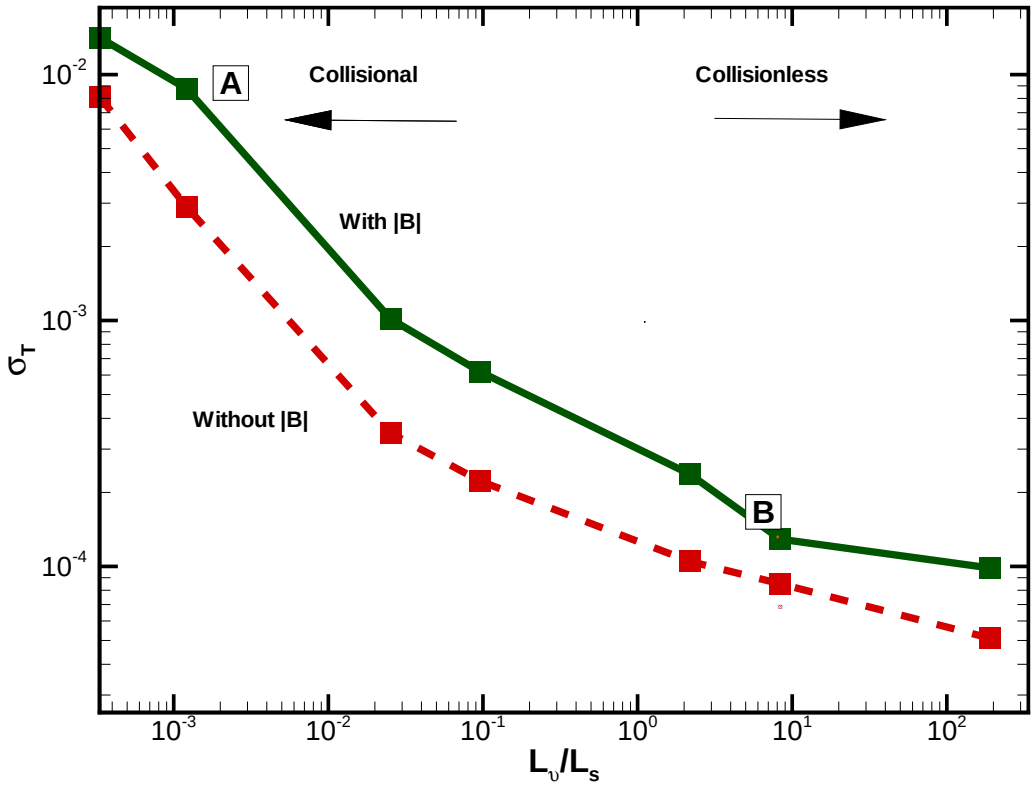


FIG. 4.5. Standard deviation in temperature in various collisionality regimes, with and without the $|\mathbf{B}|$ term in the F and T equations. As the temperature increases the standard deviation in T decreases. The presence of magnetic wells, $|\mathbf{B}|$ term, causes more fluctuations in T. Here $\delta B = 0.4$ and $L_B = 20$m. Points A in the collisional regime and B in the moderately collisional to collisionless regime, corresponds to points A and B in Figs. 4.3 and 4.4, respectively.

In the moderate collisionality regime, with collision length L_ν=10 m, the effect of $|\mathbf{B}|$ is

more easily observed in the distribution function. This arises from the terms $\underline{\mathbf{M}}v(\partial_L lnB)\mathbf{F}$ in Eq. (2.22) and $q_{||}\partial_L lnB$ in Eq. (2.17). Compared to Fig. 3.12 the presence of magnetic wells distorts the F contours more. The nonlocal behavior of the transport, as shown in Fig. 4.7, is still evident as in Fig. 3.12.

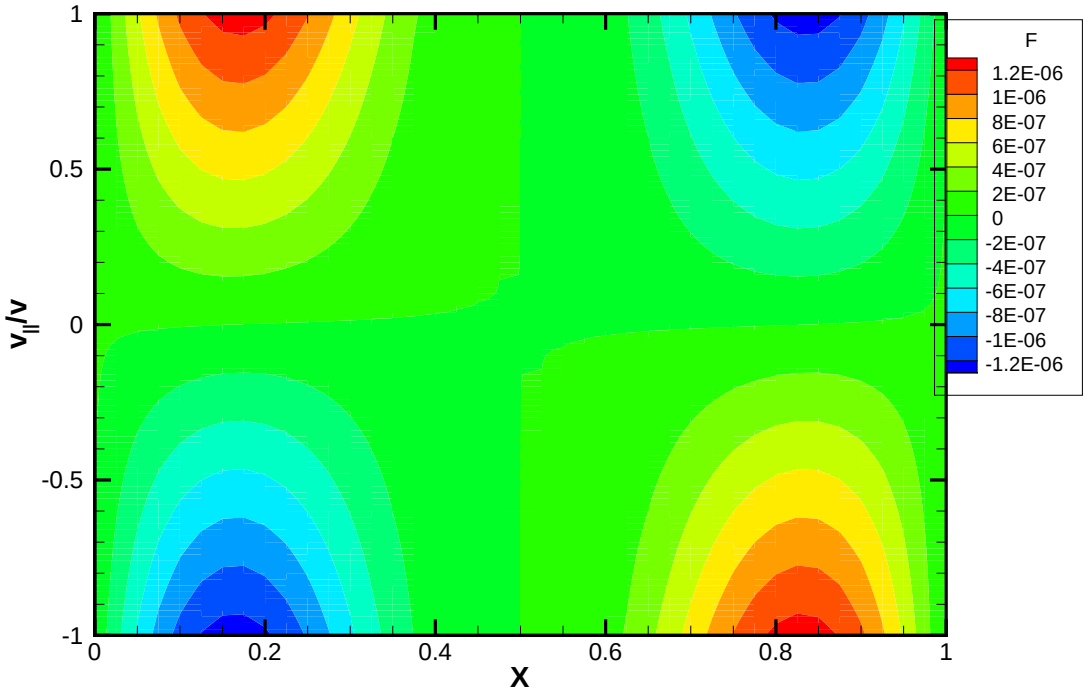


FIG. 4.6. Contours of the distribution function in the presence of magnetic wells with $\delta B = 0.4$ in the collisional regime, $L_v/L_s = 10^{-3}$. The variation in $X = L/L_{max}$ is due to the sinusoidally varying heat source. The up-down asymmetry in $v_{||}/v$ indicates the local diffusive nature of transport down the local T gradient. Compared to the case without the $|\mathbf{B}|$ effects in Figure 3.11, we see a slight distortion in the contours here.

In the nearly collisionless regime with collision length L_v=800 m, the $|\mathbf{B}|$ effects are even more apparent in the heat flow and temperature curves. When collisions are infrequent, $L_v \gg L_B$, particles execute bounce orbits and get trapped in the magnetic wells. Fig. 4.8 shows contours of the distribution function in the presence of magnetic wells with $\delta B = 0.4$. Compared to Fig. 3.13, here we see a distribution of particles near the

trapped/passing boundary (black horizontal lines at $v_{||}/v = \pm\sqrt{1-\delta B} = \pm 0.77$). A population of trapped particles is visible for $|v_{||}/v| < 0.5$. Taking into account the large temperature gradient regions shown in Fig. 4.9, we interpret the effect of magnetic wells as, in part, localizing transport along the field line making it diffusive in nature, i.e., proportional to the strong, local temperature gradient.

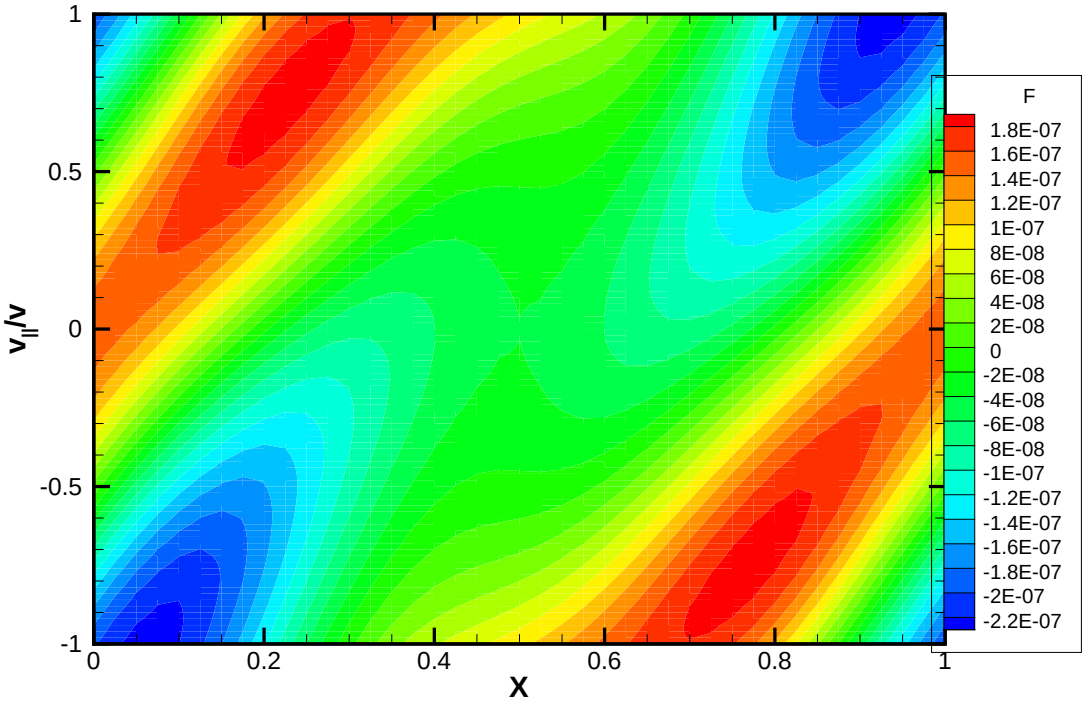


FIG. 4.7. As the frequency of collisions decreases with $L_v/L_s = 10^{-1}$, the effect of $|\mathbf{B}|$ can be observed in the contours of the distribution function for $s = 5$. The plot shows that in the presence of magnetic wells of depth $\delta B = 0.4$, the contours get distorted because of the nondiffusive, nonlocal transport arising from the free streaming, as well as from the trapping, in our kinetic equation.

Fig. 4.9 shows the temperature in the nearly collisionless regime with $\delta B = 0.4$. Considering Fig. 4.8 with this plot, it can be seen the distribution of particles is negligable in the regions where temperature gradient is 0 and is maximum where the absolute value of the gradient in T is maximum. Trapped particles do not contribute to the heat flow parallel

to the magnetic field lines over the longest scale lengths. The contours in Fig. 4.8 also show some particle distribution near the trapped/passing boundaries. To get more insight, we have plotted the distribution function weighted by $v_{||}$ in Fig. 4.10.

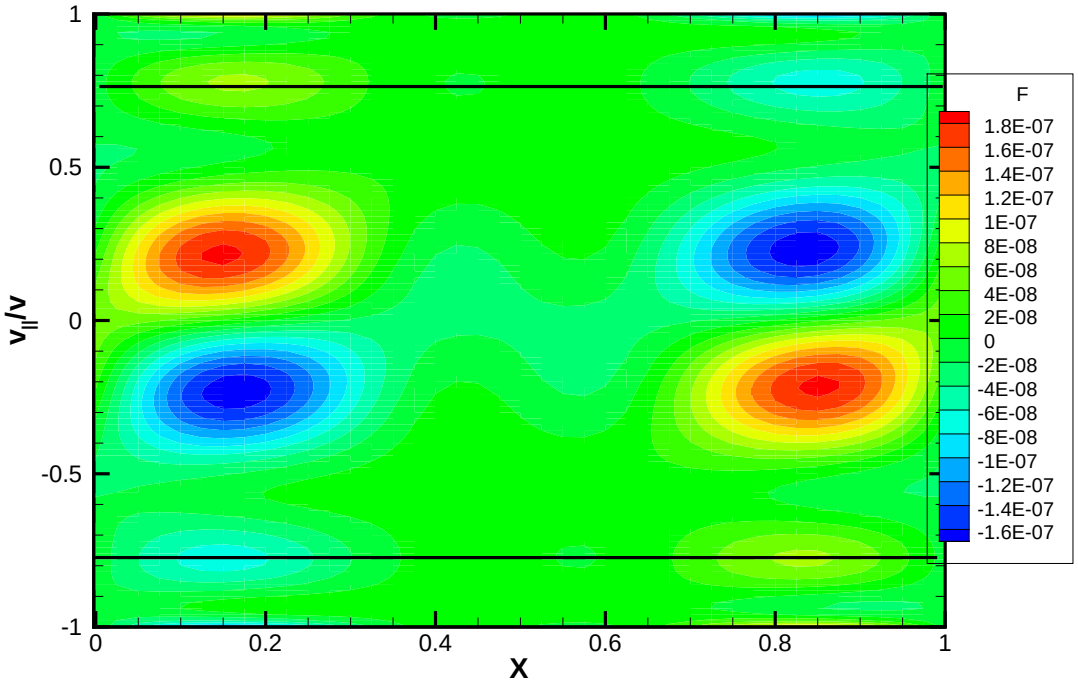


FIG. 4.8. Contours of the distribution function at $s = 5$ in the nearly collisionless regime with $L_v/L_s = 10$ in the presence of magnetic wells of well depth $\delta B = 0.4$. Here the horizontal lines represent the trapped/passing boundary. In comparision with the contours in Figure 3.13, there is a distribution of particles near the trapped/passing boundaries, but not where $v_{||}/v = 0$. We also see a distribution of trapped particles with $|v_{||}/v| < 0.5$ responding to the local temperature gradient.

Recall that $q_{||} = -T \int d\mathbf{v} v_{\|} L_1^{3/2} F$, hence the integrand of the parallel heat flow moment goes as $v_{\|} F$. The contours of the distribution function (see Fig. 4.10) weighted by $v_{||}$ indicate a similar contribution to the heat flow from particles near the trapped/passing $|v_{||}/v| = 0.77$ and from a distribution of trapped particles near $|v_{||}/v| = 0.3$. A final population near $|v_{||}/v| = 1.0$ is also apparent.

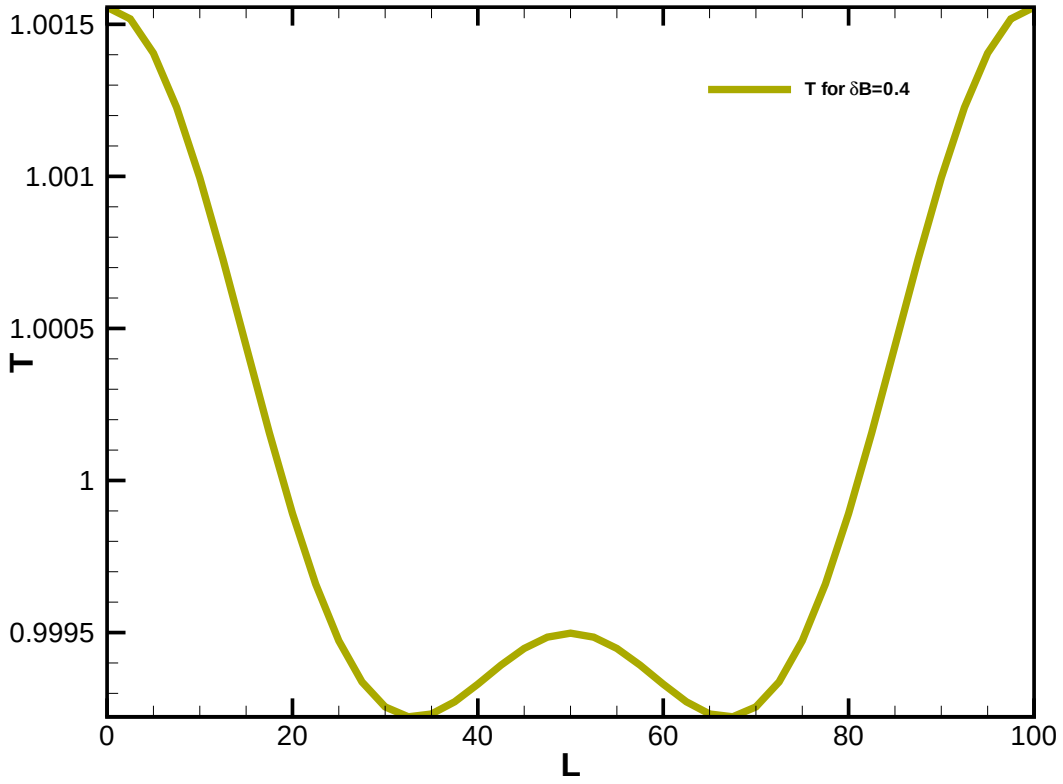


FIG. 4.9. Plot shows gradient of temperature in presence of magnetic well with $\delta B = 0.4$ in the nearly collisionless regime. A bump is observed in the temperature profile because of $|\mathbf{B}|$ effects. Also, T variations are larger over the $L_s = 100m$ scale length because only the small fraction of passing particles can carry heat over the entire domain.

4.3 Comparison of linear vs. nonlinear $|B|$ results

Recall in evaluating $\partial_L lnB$ in our kinetic and temperature equations, we used the approximate form with B_0 in the denominator of Eq. (4.2). In this section, we want to check whether using $\partial_L B/B(L)$ instead leads to substantially different predictions for σ_T. Fig. 4.11 shows a plot of σ_T in the moderate collisionality regime as affected by the magnetic well depth.

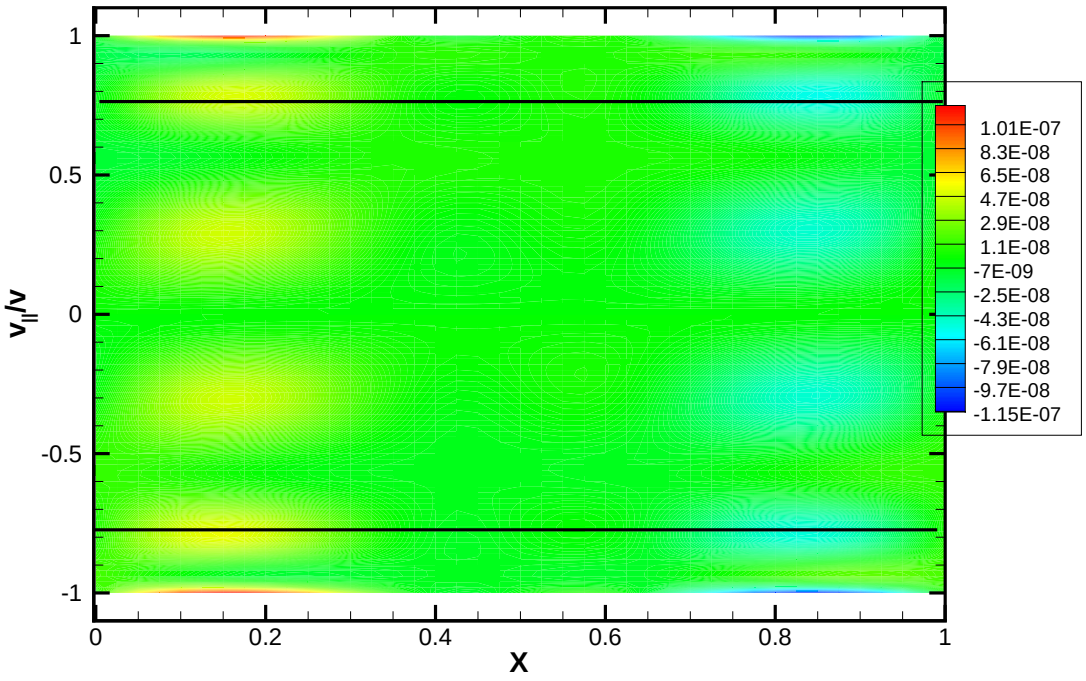


FIG. 4.10. Plot shows distribution function weighted by $v_{||}$ in the nearly collisionless regime. The $q_{||}$moment has $v_{||}F$ in the integrand. Here we see several populations in pitch-angle space contributing to the heat flow at $s = 5$.

Here the $\partial_L lnB$ term is treated using the full $B(L)$ in the denominator, represented in the red solid curve and pink dashed curve. Again, as magnetic well depth increases, the fluctuation in temperature increases. Furthermore, σ_T is larger for the case where $\partial_L lnB$ term is used in the F equation [Eq. (2.22)] indicating particles get trapped in the magnetic wells, which affects the heat flow transport parallel to the magnetic field line and ultimately the steady-state temperature. Using the full nonlinear representation of $\partial_L lnB$ term slightly increases the fluctuations in the temperature and brings into question the linearized $\partial_L lnB$ treatment when $\delta B \geq 0.4$. For the result presented in this work, however, the linear approximation to $\partial_L lnB$ is accurate.

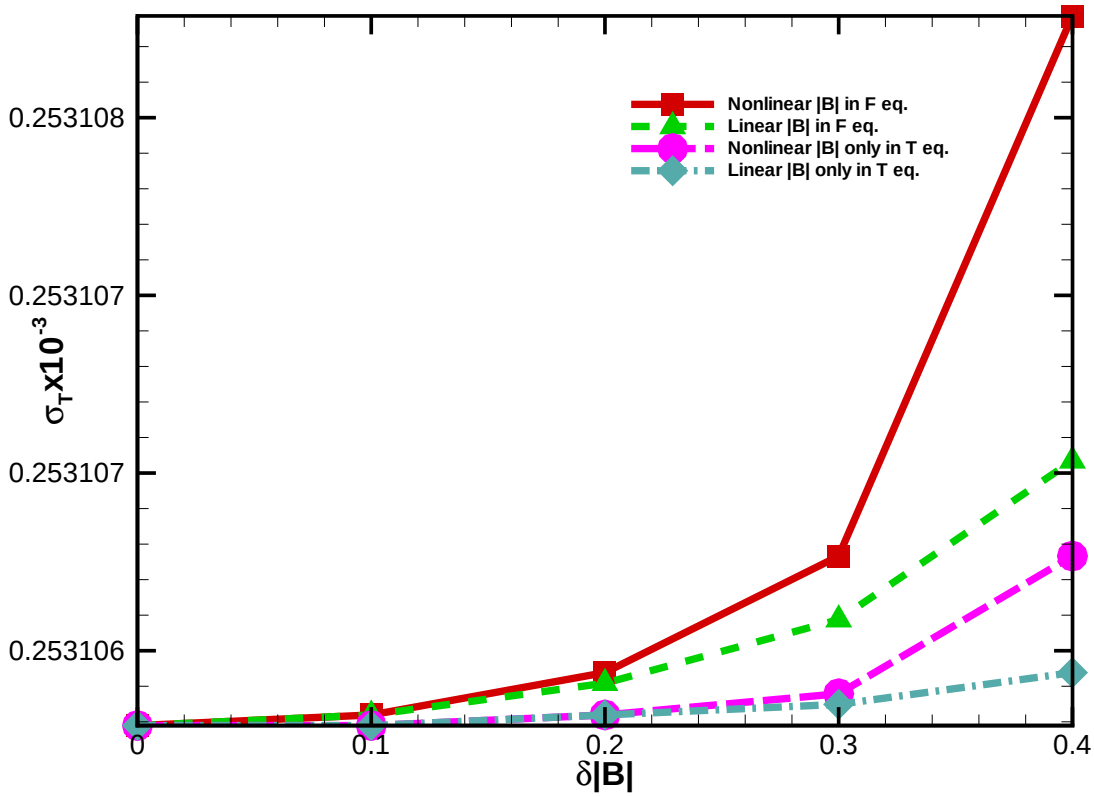


FIG. 4.11. Plot of standard deviation in temperature in moderate collisionality regime versus magnetic well depth with and without the affect of $\partial_L lnB$ term in our kinetic equation. In the red solid curve and pink dashed curve, the full B dependence is used in evaluating the denominator of $\partial_L lnB$ with red corresponding to $|\mathbf{B}|$ in the F and T equations and pink to $|\mathbf{B}|$ in the T equation only. Note the full $B(L)$ dependence in the denominator leads to slightly larger T variation along field lines.

CHAPTER 5

CONCLUSIONS AND FUTURE WORK

In this chapter we focus on summarizing the key results obtained in this work, as well as on the research path to follow in the future. The focus of this work was to incorporate kinetic physics via a closure for the parallel electron heat flow into the evolution of electron temperature. A Fortran code was written to solve the coupled kinetic/temperature PDE system in an efficient manner. Computational studies were completed to understand parallel heat transport in different collisionality regimes for magnetized plasmas.

A hybrid fluid-kinetic approach was used and the Chapman-Enskog Ansatz was applied to derive the lowest-order, time-dependent CEL drift kinetic equation (CEL-DKE). The CEL-DKE was then simplified to address the coupled kinetic/temperature system and the kinetic distortion, F, was expanded in Legendre polynomials parameterized by $v_{||}/v$. The temperature evolution equation was coupled to the F equation and the system was solved for the kinetic distortion, whose velocity moment was taken to obtain the generalized parallel electron heat flow closure, $q_{||}$. In this work, the Lorentz collision operator was used, and results were obtained for various collisionality regimes. The analytical model was then implemented in a Fortran code for studying the effects of collisionality and particle trapping on the heat flow along magnetic field lines. Results presented in Chapters 3 and 4 show the dependence of the steady-state temperature on collisionality and magnetic well depths.

5.1 Summary of the results

The results obtained in this work can be divided into three important parts. One part is comprised of convergence studies, which are important in order to obtain computationally accurate results. Another part (Chapter 3) contains a study of the effect of collisionality on heat transport and the steady-state temperature variations along magnetic field lines. The

final part (Chapter 4) explored the effect of magnetic wells and particle trapping on the steady-state distribution function and temperature.

The accuracy of the computationally obtained results relies on numerical convergence of our treatment of the coupled kinetic/temperature system. In this work we check for convergence of the truncated Legendre polynomial expansion for F which included N terms and convergence in the number of speed points, n_s, which were assigned to separate processors in order to quickly reach the steady state. We check for convergence by studying the effect of these parameters on temperature fluctuations in various collisionality regimes. The key results obtained in achieving numerical convergence and in studying the effects of collisionality and particle trapping are stated below.

- The number of terms in the expansion of F depends on the number of Legendre polynomials, N. In collisional regimes, fewer Legendre polynomials are required and convergence of the standard deviation in temperature, σ_T, is achieved even with $N = 2$. This result agrees with previous work present in the literature. In nearly collisionless regimes, σ_T decreases with increasing number of Legendre polynomials and converges for $N = 16$. More Legendre polynomials are required for the nearly collisionless case because the structure in pitch angle, $v_{||}/v$, becomes more complex. This is due to the fact details in pitch-angle are not destroyed completely by the weak pitch-angle scattering process.

- In order to cut down on computational time for scans in the number of speed grid points, n_s, separate processors are assigned their own s value. Convergence in speed points is checked by studying the behavior of σ_T as n_S is increased for various collisionality regimes. In the collisional regime, convergence is rapidly achieved for $n_S = 5$. In the nearly collisionless regime, it is difficult to show uniform convergence, since at high temperature, it is difficult to achieve a true steady-state without fluctuations in time. We speculate an improved collision operator with speed dif-

fusion and drag effects might aid convergence studies in n_s in nearly collisionless plasmas.

- In the absence of magnetic wells, frequent collisions lead to heat flow proportional to the local parallel gradient of temperature with the direction of $q_{\|}$ down the local temperature gradient. As the background temperature increases, variations in T are reduced since more energetic electrons are able to smooth out temperature perturbations along the field lines. As the background temperature approaches 1Kev, reduction in σ_T slows due to the flux-limited transport effect. In the presence of magnetic wells, temperature variations increase. Recall in this work, no constraint is applied to order the scale length of magnetic wells compared to temperature scale lengths. Temperature variations increase for deeper magnetic wells due to both the squeezing effect of heat flow in the T equation and due to the trapping of electrons in local magnetic wells.

- As the collisionality decreases, σ_T decreases. However, σ_T increases with increasing magnetic well depth, since more particles are trapped in magnetic wells. In the collisional regime, a purely fluid effect is observed with $q_{\|}$ being squeezed by variations in $|\mathbf{B}|$. In moderately collisional to collisionless regimes, passing/trapped particles are influenced by magnetic wells, i.e, the $|B|$ term, as evidenced by the $v_{\|}$-weighted contours in Fig. 4.10 at the end of Chapter 4.

- We have solved the coupled system of the CEL-DKE and temperature evolution equations and studied the steady-state distribution function, F. Several contour plots were presented to better understand the dynamics in our 2D velocity space. In the collisional regime, there are equal number of particles moving in opposite directions at a given time. Transport is mainly diffusive in nature and does not get affected much by the presence of magnetic wells. In moderate collisionality regimes, nonlocal transport comes into play, and the presence of magnetic wells becomes important.

In this regime, particles carrying heat in opposite directions are not exactly opposite to each other in space. In the high-temperature regime, a reduced population of passing particles move freely along field lines, while a larger population of particles are trapped in magnetic wells.

- We have also determined using the full, nonlinear $\partial_L lnB$ in our kinetic and temperature equations increases σ_T in comparison to the linear cases which used the constant B_0 in the denominator. While this effect was slight for $\delta B < 0.4$, we note for cases with $\delta B > 0.4$, it would be necessary to include the full $B(L)$ in the denominator.

5.2 Future work

5.2.1 Improved collision operator for electrons

The physical effects of collisions of particles in ionized fusion plasmas are best treated using the full Coulomb collision operator as opposed to the simplified Lorentz form. In our work, the physics of particle diffusion in pitch-angle space is represented by the Lorentz pitch-angle scattering operator defined in Eq. (2.5). As an important extension to our work, we suggest including the speed diffusion and drag portions of the Coulomb collision operator.

A form of the linearized, Coulomb collision operator that assumes a small mass ratio ($m_e/m_i << 1$) is the following moment form:

$$C_e^{(1)} = \sum_a [\frac{-\nu_{Lea}}{2} \sum_{n=1}^{N} n(n+1) P_n \left(\frac{v_{||}}{v}\right) F_n + \sum_{k\geq 1} \frac{f_{M_a}}{\sigma_k^1} P_1 \left(\frac{v_{||}}{v}\right) M_{||a}^{1k} \nu_{ea}^{1k}] + f_{M_a} \frac{\nu_{ei}}{s_e^2} P_1 \left(\frac{v_{||}}{v}\right) (V_{||_i} - V_{||_e}). \quad (5.1)$$

Here, $(V_{||_i} - V_{||_e})$ is the difference in the parallel ion and electron flows, each normalized to their respective thermal speeds. The $k = 1$ moment, $M_{||a}^{1k}$, is related to the parallel heat flow closure, $q_{||}$. This form allows for speed diffusion and drag, as well as momentum exchange, between flowing electron and ion species. Note the first term is the Lorentz

operator used in this work. Implementation of this electron collision operator in our code would be tedious but straightforward.

5.2.2 Full (nonlinear) temperature

In this research, we have normalized temperature to a constant background temperature, T_0, in solving our system of coupled equations for $q_{||}$. Future research could target incorporating the full temperature into our equations. Full temperature means using $T(L)$ everywhere as opposed to just in the thermodynamic drive term, $\partial_L T$. In section 2 temperature is defined as

$$T = T_0 + \sum_{m>0}^{m_{max}} (T_m e^{im\phi} + T_m^* e^{-im\phi}).$$

By substituting the full $T(L)$ into the F and T equations, we can write the dedimensionalized CEL-DKE as

$$[\underline{\mathbf{I}}\partial_{\bar{t}} + \frac{\nu_L}{2(v_0/L_0)}\Gamma]\mathbf{F} + \sqrt{\bar{T}}s[\underline{\mathbf{A}}\partial_{\bar{L}} + \underline{\mathbf{M}}\partial_{\bar{L}} lnB]\mathbf{F} \quad = \quad \delta_{l1} L_1^{\frac{3}{2}} \frac{e^{-s^2}}{\pi^{\frac{3}{2}}} s \frac{v_{||}}{v} \frac{\partial_L \bar{T}}{\bar{T}^2}. \tag{5.2}$$

The temperature evolution equation becomes

$$\partial_{\bar{t}} \bar{T} = \frac{8\pi}{9} \bar{T}^3 [\int ds s^3 L_1^{\frac{3}{2}} [\partial_{\bar{L}} + \partial_{\bar{L}} lnB] F_1 + \bar{S}, \tag{5.3}$$

where $\partial_{\bar{t}} = \frac{L_0}{v_0}\partial_t$, $\partial_{\bar{L}} = \partial_{L/L_0}$, and $\mathbf{F} = \frac{v_0^3}{n}\mathbf{F}$ with normalized temperature $\bar{T} = \frac{T}{T_0}$.

With this definition of temperature we can write the full (nonlinear) temperature term $\partial_{\bar{L}}\overline{T}/\overline{T}^2$ in our F equation as

$$\partial_{\bar{L}}\overline{T} \quad /\overline{T}^2 = \quad \frac{1}{\overline{T}^2(\bar{L})}\partial_{\bar{L}} T = \frac{\sum_{m>0}^{m_{max}} \left(im\frac{2\pi}{\bar{L}_{\overline{T}}} \right) (\overline{T}_m e^{im\phi} - \overline{T}_m^* e^{-im\phi})}{(1 + \sum_{m>0}^{m_{max}} (\overline{T}_m e^{im\phi} + \overline{T}_m^* e^{-im\phi}))^2}. \tag{5.4}$$

By not using the full temperature dependence in our research, it has been hard to get results in the nearly collisionless case for magnetic well depths $\delta B > 0.4$. Use of the full

temperature would allow studies of more extreme δB (on the order of, but less than 1) with stronger heat sources in higher-temperature plasmas. Preliminary work on such studies is underway.

REFERENCES

[1] Z. Chang and J. D. Callen, Phys. Fluids B: Plasma Phys. **4**, 1167 (1992).

[2] Z. Chang and J. D. Callen, Phys. Fluids B: Plasma Phys. **4**, 1182 (1992).

[3] J. P. Wang and J. D. Callen, Phys. Fluids **4**, 1139 (1992).

[4] R. Landshoff, Phys. Rev. **76**, 904 (1949).

[5] L. Spitzer and R. Härm, Phys. Rev. Lett. **89**, 979 (1953).

[6] M. N. Rosenbluth and A. N. Kaufman, Phys. Rev. **109**, 1 (1958).

[7] S. I. Braginskii, *Transport Processes in a Plasma*, Vol. 1 (edited by M. A. Leontovich, New York, 1965).

[8] G. W. Hammett and F. W. Perkins, Phys. Rev. Lett. **64**, 3019 (1990).

[9] E. D. Held, Phys. Plasmas **10**, 4708 (2003).

[10] E. D. Held, J. D. Callen, C. C. Hegna, and C. R. Sovinec, Phys. Plasmas **8**, 1171 (2001).

[11] E. Held, J. Callen, and C. Hegna, Phys. of Plasmas **10**, 3933 (2003).

[12] H. Grad, Phys. Today **22**, 34 (1969).

[13] H. Grad, Comm. on Pure and Applied Math. **2**, 331 (1949).

[14] G. F. Chew, M. L. Goldberger, and F. E. Low, Proc. Royal Society of London. Series A, Mathematical and Physical Sciences **236**, pp. 112 (1956).

[15] E. L. Vold, F. Najmabadi, and R. W. Conn, Phys. Fluids B: Plasma Phys. **3**, 3132 (1991).

[16] S. Chapman and T. G. Cowling, *The Mathematical Theory of Non-Uniform Gases* (Cambridge University Press, Cambridge, 1939).

[17] J. A. Bittencourt, *Fundamentals of Plasma Physics* (Springer, New York, 2004).

[18] S. Friedlander and D. Serre, *Handbook of Mathematical Fluid Dynamics* (Elsevier, Amsterdam; Boston, 2002-2004).

[19] D. C. Montgomery, *Plasma kinetic theory* (McGraw-Hill, New York, 1964).

[20] R. D. Hazeltine, Plasma Phys. **15**, 77 (1973).

[21] C. F. Delale, J. Stat. Phys. **28**, 589 (1982).

[22] R. A. Koch and J. Wendell Horton, Phys. Fluids **18**, 861 (1975).

[23] S. Chandrasekhar, Revs. Modern Phys. **15**, 1 (1943).

[24] W. Gropp, *Using MPI [electronic resource] : portable parallel programming with the message-passing interface* (MIT Press, Cambridge, 1999).

[25] J. Candy and R. Waltz, J. Comput. Phys. **186**, 545 (2003).

[26] C. Estrada-Mila, J. Candy, and R. E. Waltz, Phys. of Plasmas **12**, 022305 (2005).

[27] S. I. Krasheninnikov, Phys. Fluids B **5**, 74 (1993).

[28] J. A. Krommes, Phys. Plasmas **6**, 1477 (1999).

APPENDIX

A.1 Properties of Legendre polynomials

Legendre polynomials are solutions to Legendre's differential equation :

$$\frac{d}{dx}\left[(1-x^2)\frac{d}{dx}P_n(x)\right]+n(n+1)P_n(x)=0. \tag{5.5}$$

An important property of the Legendre polynomials is their orthogonality on the interval $-1 \leq x \leq 1$:

$$\int_{-1}^{1} P_m(x)P_n(x)dx = \frac{2}{2n+1}\delta_{mn}. \tag{5.6}$$

Here $\delta_{mn} = \begin{cases} 0 & if\ m \neq n \\ 1 & if\ m = n \end{cases}$ is the Kronecker delta.

Additional properties of the Legendre polynomials used in this research (Chapter 2) are the following recurrence relations :

$$(x^2-1)\frac{d}{dx}P_n(x) \quad = \quad nxP_n(x) - nP_{n-1}(x), \tag{5.7}$$

and

$$(n+1)P_{n+1}(x) \quad = \quad (2n+1)xP_n(x) - nP_{n-1}(x). \tag{5.8}$$

A.2 Definition of Laguerre polynomials

Laguerre polynomials are defined either by the series representation :

$$L_n^{\alpha}(x) = \frac{(-x)^m\Gamma(n+\alpha+1)}{m!(n-m)!\Gamma(m+\alpha+1)}, \tag{5.9}$$

or by Rodrigue's representation :

$$L_n^{\alpha}(x) = \frac{1}{n!} e^x x^{-\alpha} \frac{d^n}{dx^n}(e^{-x} x^{n+\alpha}). \tag{5.10}$$

The first three lowest-order Laguerre polynomials are :

$L_0^{\alpha}(x) = 1,$

$L_1^{\alpha}(x) = \alpha + 1 - x,$

and

$L_2^{\alpha}(x) = \frac{(\alpha+1)(\alpha+2)}{2} - (\alpha+2)x + \frac{x^2}{2}.$

A.3 Derivation of |B| coupling terms

Given the definition $\frac{v_{||}(L)}{v} = \pm\sqrt{1 - \frac{\mu B(L)}{w}}$, we compute

$$\frac{d}{dL} P(\frac{v_{||}(L)}{v}) = \frac{d}{dL}\left(\frac{v_{||}(L)}{v}\right) \frac{d}{dL} P\left(\frac{v_{||}(L)}{v}\right) = \pm \frac{1}{2\sqrt{1 - \frac{\mu B(x)}{w}}} (-\frac{\mu B}{w})(\partial_L ln B) P^{'}$$

$$\frac{d}{dL}\left(\frac{v_{||}(L)}{v}\right) = \frac{d}{dL}\left[\pm\sqrt{1 - \frac{\mu B(L)}{w}}\right] \tag{5.11}$$

$$\frac{d}{dL}\left(\frac{v_{||}(L)}{v}\right) = \pm \frac{1}{2\sqrt{1 - \frac{\mu B(L)}{w}}} (-\frac{\mu B}{w})(\partial_L ln B)$$

$$\frac{d}{dL}\left(\frac{v_{||}(L)}{v}\right) = -\frac{1}{2\left(\frac{v_{||}}{v}\right)} \left[\left(\frac{v_{||}}{v}\right)^2 - 1\right] (\partial_L ln B)$$

$$\int_{-1}^{1} d(\frac{v_{||}}{v}) P_m\left(\frac{v_{||}}{v}\right)\left[n\left(\frac{v_{||}}{v}\right)P_n - nP_{n-1}\right] =$$
$$\left[\frac{n(n+1)}{(2n+1)(2n+3)}\delta_{m,n+1} - \frac{n(n+1)}{(2n+1)(2n-1)}\delta_{m,n-1}\right].$$

This term leads to coupling of our expansion coefficients for the Legendre polynomials. Physically, it contains the effects of trapped and passing particles in velocity space.

CURRICULUM VITAE

Mukta Sharma
(November 2012)

772 North 750 East, Apt 3
Logan, UT 84321

(435) 512-7919
mukta.sharma@aggiemail.usu.edu

EXPERTISE

- Analytical and numerical methods to enhance plasma theory.
- Advancing plasma kinetic theory and related computational algorithms and associated data analysis tools.
- Implementing methods for closing the plasma fluid temperature equation.
- Extensive use of Fortran 90 and other programming/scripting languages.
- Use of libraries like SuperLU, IMSL and MPI for solving sparse, non-symmetric systems of equations.

EDUCATION

Ph.D. Physics December 2012	**Utah State University**, Logan, UT Physics. GPA: 3.81 Dissertation: *Parallel heat flow transport in magnetized plasma.* Major Professor: Eric D. Held
M.S. May 2002	**University of Delhi,** Delhi, India Physics (Specialization in Experimental Solid State Physics)
B.S. May 2000	**University of Delhi,** Delhi, India Physics (Honors)

COMPUTER SKILLS

- Programming Languages: FORTRAN, C, HTML, Pascal
- Operating Systems: Linux, Windows, Mac OS X
- Windows Applications: Word, Excel, PowerPoint, Access
- Scientific Applications: Tecplot, Maple, IGOR
- Scripting Languages: LyX, LaTeX

EXPERIMENTS AND PROJECTS

- Design and construction of Hall's coefficient experiment (GaAs) for advanced Solid State Physics Lab.
- Critical temperature experiment for high temperature superconductor.
- Design and construction of spray pyrolysis unit for thick film growth of high temperature superconductor.
- Thick film and bulk growth of high temperature superconducting materials.
- Analysis of surface core level shifts W(110).

WORK EXPERIENCE

Graduate Research Assistant (May 2005– present)

Utah State University Logan, Utah

- Closing the fluid equations and advancing plasma kinetic equations with analytical and numerical methods.
- Using techniques like implicit and explicit time discretization for obtaining time dependent numerical solutions of plasma equations.

- Using Fast Fourier Transform algorithm for research.
- Using methods like Gaussian quadrature for solving definite integrals.
- Experience in using libraries like SuperLU, IMSL and MPI for solving sparse, non-symmetric systems of equations.
- Solving ordinary and partial differential equations.
- Experience in writing and running FORTRAN and Maple code.
- Significant experience using LyX and Tecplot.

Graduate Teaching Assistant (Spring 2010-Spring 2011)

Utah State University Logan, Utah

- Taught undergraduate labs for up to 20 students in engineering and pre-med.
- improved student's interpersonal and problem solving skills by holding weekly homework help sessions.

Research Fellow (Summer 2002-Summer 2004)

University of Delhi and National Physical Laboratory, India

- Synthesis, analysis and characterization of bulk, thin film YBCO/BSCCO.
- Design and construction of low temperature cryostat (77 Kelvin).
- Proficient in design and operation of DC Sputtering system.
- Magneto-resistance techniques to study the effect of defects.
- Operation of high temperature furnaces.

- Hydraulic pressure dyes.
- Low temperature measurements (77 Kelvin).

PRESENTATIONS

2011	**Parallel electron heat flow closure in in-homogeneous magnetic field** *Mukta Sharma, E.D. Held, NIMROD Team Meeting, Logan, Utah, 2011*
2010	**Parallel heat flow closure for toroidal plasmas** *Mukta Sharma, E.D. Held, J.Y. Ji, American Physical Society, Four Corners Meeting, Ogden, Utah, 2010*
2009	**Neoclassical parallel closures for toroidal plasmas** M*ukta Sharma, E.D. Held, J.Y. Ji, 51st Annual Meeting Of The American Physical Society, Atlanta, Georgia, 2009*
2009	**Parallel heat flux and stress tensor in toroidal plasmas** *Mukta Sharma, E.D. Held, Intermountain Graduate Research Symposium, Logan, Utah, 2009*
2008	**Parallel heat flow and stress tensor in toroidal plasmas** *Mukta Sharma, E.D. Held, J.Y. Ji, 50th Annual Meeting of the American Physical Society, Dallas, Texas, 2008*
2006	**General parallel closures for tokamak plasmas** *M. Sharma, J.Y. Ji, E.D. Held, American Physical Society, Four Corners Meeting, Logan, Utah, 2006*
2005	**Epitaxial growth of Au on W(110): analysis of core level shifts and line shapes** *Mukta Sharma, D.M. Riffe, American Physical Society, Four Corners Meeting, Boulder, Colorado, 2005*

HONORS

- Lawrence R. and Abelina Megill Scholarship (2006), Department of Physics, Utah State University, Logan, Utah
- Joint CSIR-UGC National Eligibility Test (NET) for Lectureship (2004), Council of Scientific and Industrial Research, New Delhi, India

PROFESSIONAL AFFILIATIONS

- Sigma Pi Sigma
- American Physical Society